



## Division and Adaptation to Host Environment of Apicomplexan Parasites Depend on Apicoplast Lipid Metabolic Plasticity and Host Organelle Remodeling

Souad Amiar, Nicholas Katris, Laurence Berry, Sheena Dass, Samuel Duley, Christophe-Sebastien Arnold, Melanie Shears, Camille Brunet, Bastien Touquet, Geoffrey Mcfadden, et al.

### ► To cite this version:

Souad Amiar, Nicholas Katris, Laurence Berry, Sheena Dass, Samuel Duley, et al.. Division and Adaptation to Host Environment of Apicomplexan Parasites Depend on Apicoplast Lipid Metabolic Plasticity and Host Organelle Remodeling. Cell Reports, 2020, 30 (11), pp.3778-3792.e9. 10.1016/j.celrep.2020.02.072 . hal-03103818

**HAL Id: hal-03103818**

**<https://hal.science/hal-03103818>**

Submitted on 22 Aug 2022

**HAL** is a multi-disciplinary open access archive for the deposit and dissemination of scientific research documents, whether they are published or not. The documents may come from teaching and research institutions in France or abroad, or from public or private research centers.

L'archive ouverte pluridisciplinaire **HAL**, est destinée au dépôt et à la diffusion de documents scientifiques de niveau recherche, publiés ou non, émanant des établissements d'enseignement et de recherche français ou étrangers, des laboratoires publics ou privés.



Distributed under a Creative Commons Attribution - NonCommercial 4.0 International License

**Division and adaptation to host environment of apicomplexan parasites  
depend on apicoplast lipid metabolic plasticity and host organelles  
remodelling**

Running Title: Apicomplexa lipid synthesis controls division and metabolic adaptation

Souad Amiar<sup>1+</sup>, Nicholas J. Katris<sup>1+</sup>, Laurence Berry<sup>2</sup>, Sheena Dass<sup>1</sup>, Duley Samuel<sup>1</sup>,  
Arnold Christophe-Sebastien<sup>1</sup>, Melanie J. Shears<sup>3</sup>, Camille Brunet<sup>1</sup>, Bastien  
Touquet<sup>4</sup>, Geoffrey I. McFadden<sup>3</sup>, Yoshiki Yamaryo-Botté<sup>1, #, \*</sup>, Cyrille Y. Botté<sup>1 #, @, \*</sup>

<sup>1</sup> ApicoLipid Team, Institute for Advanced Biosciences, CNRS UMR5309, Université  
Grenoble Alpes, INSERM U1209, Grenoble, France,

<sup>2</sup> Dynamique des interactions Membranaires normales et pathologiques, UMR5235,  
Université MontpellierII, France.

<sup>3</sup> McFadden Laboratory, School of Biosciences, University of Melbourne, VIC 3010,  
Australia.

<sup>4</sup> Team Cell and membrane dynamics of parasite-host interaction, Institute for  
Advanced Biosciences, INSERM 1209, CNRS UMR5309, Université Grenoble Alpes,  
France

+ These authors contributed equally

# Senior Author

@ Lead Contact

\* \* Correspondance: [cyrille.botte@univ-grenoble-alpes.fr](mailto:cyrille.botte@univ-grenoble-alpes.fr) / [cyrille.botte@gmail.com](mailto:cyrille.botte@gmail.com) ;  
[yoshiki.yamaryo@gmail.com](mailto:yoshiki.yamaryo@gmail.com)

**Keywords:** Apicomplexa, toxoplasmosis, malaria, apicoplast, lipid synthesis, phosphatidic acid, host-parasite interaction, lipidomics, host nutritional environment, cytokinesis

**Abstract:**

Apicomplexan parasites are unicellular eukaryotic pathogens and must obtain and combine lipids both from host cell scavenging and *de novo* synthesis to maintain parasite propagation and survival within their human host. Major questions on the role for, and regulation of, each lipid source upon fluctuating host nutritional conditions remain unanswered. Characterization of an apicoplast acyltransferase *TgATS2*, shows that the apicoplast provides (lyso)phosphatidic acid, required for the recruitment of a critical dynamin (*TgDrpC*) during parasite cytokinesis. Disruption of *TgATS2* also led parasites to shift metabolic lipid acquisition from *de novo* synthesis towards host scavenging. We uncover that both lipid scavenging and *de novo* synthesis pathways in wild-type parasites exhibit major metabolic and cellular plasticity upon sensing host lipid-deprived environments through concomitant (i) up-regulation of *de novo* fatty acid synthesis capacities in the apicoplast, and (ii) parasite-driven host remodelling to generate multi-membrane-bound structures from host organelles that are imported towards the parasite.

**Highlights:**

- Knockout of apicoplast *TgATS2* disrupts LPA/PA for DrpC recruitment during cytokinesis
- *T. gondii* can sense host environment and adapt to low host nutritional content
- Under lipid starvation, parasite *FASII* and other lipid metabolic genes become essential

- Upon nutrient deprivation, *T.gondii* induces host organelle remodelling and vesiculation

## eTOC Blurb

Apicoplast de novo lipid synthesis and lipid host scavenging are both critical for apicomplexan intracellular development. Amiar and Katris et al. show that the parasite adapts to the fluctuations of host nutritional content to regulate the metabolic activity of both apicoplast and scavenging pathways and maintain parasite development and division.

Apicoplast de novo lipid synthesis and lipid host scavenging are both critical for apicomplexan intracellular development. Amiar and Katris et al. show that parasites adapt to fluctuations of host nutritional content to regulate the metabolic activity of both apicoplast and scavenging pathways to maintain parasite development.

## Introduction:

Apicomplexa are intracellular protozoan parasites that cause serious infectious diseases in humans including malaria, and toxoplasmosis. Most Apicomplexa harbour a relict non-photosynthetic plastid, the apicoplast, acquired by the secondary endosymbiosis of a red alga (Janouskovec et al., 2010). The apicoplast lost photosynthetic capability during the conversion to a parasitic lifestyle (Botte et al., 2013). However, it still contains plant-like pathways including a prokaryotic type II fatty acid synthesis pathway (FASII) (Waller et al., 1998). The apicoplast is essential for parasite survival in both *T. gondii* and *P. falciparum* (MacRae et al., 2012).

However the FASII pathway is thought to be essential only during specific life stages. Indeed in *Plasmodium*, disruption of FASII was demonstrated to be dispensable in asexual blood stages but essential for late liver stage in rodent malaria parasites, and



for sporozoite schizogony during mosquito stages (Vaughan et al., 2009). Nevertheless, changes in *P. falciparum* blood stage growth conditions—such as lipid starvation during *in vitro* growth, or physiological stress in human patients—induced re-activation of apicoplast FASII (Daily et al., 2007, Botte et al., 2013), suggesting plasticity of the FASII in response to nutritional environment. In *T. gondii*, FASII is essential during tachyzoite development (Mazumdar et al., 2006).

Apicomplexan parasite membranes comprise up to 80% phospholipid (PL) as a proportion of total lipid classes, primarily phosphatidylcholine (PC), phosphatidylethanolamine (PE), phosphatidylserine (PS) and phosphatidylinositol (PI, (Welti et al., 2007, Gulati et al., 2015). *T. gondii* can readily scavenge PL, and triacylglycerols (TAG) from the host but is also capable of-, and dependent on- *de novo* synthesis of several PL classes (Hu et al., 2017, Amiar et al., 2016, Nolan et al., 2017). Like other eukaryotes, apicomplexan *de novo* PL synthesis is initiated by the assembly of FA (i.e. esterification onto a glycerol-phosphate backbone) into specific PL precursors. In *T. gondii*, FAs to be integrated into PLs derive from three sources: (i) apicoplast FASII generating FA chains (C12:0, C14:0, and C16:0) (Ramakrishnan et al., 2012), (ii) FA elongases located on the parasite endoplasmic reticulum (ER; C16:1, C18:1, C20:1, C22:1 and C26:1) (Dubois et al., 2018), and (iii) FAs scavenged from the host cell (Bisanz et al., 2006). Lipidomics reveals that most *T. gondii* PLs are hybrid/patchwork molecules, comprising one FA moiety from the apicoplast *de novo* synthesis pathway and a second one scavenged from the host (Amiar et al., 2016). Thus, both scavenging and *de novo* synthesis of FA are critical for intracellular development.

Typically, phosphatidic acid (PA) is the central precursor for the *de novo* synthesis of all PL classes by the two-step esterification of FAs onto a glycerol-3-phosphate

98 backbone; first by glycerol-3-phosphate acyltransferases (GPAT) to form  
99 lysophosphatidic acid (LPA), and then by acyl-glycerol-3-phosphate  
100 acyltransferases (AGPAT) to convert LPA to PA. In eukaryotic cells, GPATs and  
101 AGPATs of diverse origins that work as a set at several locations within the cell.  
102 Apicomplexans have two sets of acyltransferases: one plastid-like set putatively in  
103 the apicoplast (prokaryotic pathway), (Amiar et al., 2016) and another pair predicted  
104 to be in the ER (so-called eukaryotic pathway). In *T. gondii* the apicoplast GPAT,  
105 *TgATS1*, is essential for tachyzoite development where it generates LPA from  
106 apicoplast-FA for the bulk synthesis of PL (Amiar et al., 2016). The role of parasite  
107 AGPATs for lipid synthesis is yet to be determined. Beyond their roles as lipid  
108 precursors, PA (and LPA) also have important biophysical properties by controlling  
109 the formation of positive or negative membrane curvatures, and thereby influence the  
110 recruitment of proteins involved in membrane fusion/fission events such as  
111 endocytosis in other eukaryotic models (Schmidt et al., 1999, Kooijman et al., 2005,  
112 Brown et al., 2008).

113 Here we characterise *T. gondii* AGPATs, focusing on one (*TgATS2*) localized to the  
114 apicoplast. We confirm that *TgATS2* is an acyltransferase by complementing a  
115 bacterial mutant, and we construct a knockout mutant in which we observe the  
116 defects in parasite cytokinesis, and the parasite lipid profile. Particularly, the impact  
117 of LPA/PA changes on the localization of a dynamin-related protein, *TgDrpC*, in the  
118 *TgATS2* mutant is described and provides a rationale for cytokinesis defects  
119 associated with drug inhibition of apicoplast FASII (Martins-Duarte et al., 2015).  
120 Finally, changes in parasite lipid composition and lipid fluxes led us to subject  
121 parasites to lipid starvation to explore how host nutritional environment impacts  
122 parasite growth. Analysis of lipid fluxes and growth screening under adverse lipid

conditions show that parasites can sense the environment and respond by (i) upregulation of *de novo* lipid synthesis in the apicoplast and (ii) manipulation of the human host through vesiculation from host organelles and import of such material to the parasitophorous vacuole (PVM) mediated by export of parasite effectors to improve their lipid scavenging. Our analysis provides unprecedented mechanistic insights into parasite metabolic adaption under host nutritional challenge, which was poorly understood until now.

## Results

### **Deletion of *Toxoplasma gondii* apicoplast acyltransferase *TgATS2* results in aberrant cytokinesis and residual body formation during replication.**

To explore *de novo* PA synthesis in *T. gondii*, we searched the genome for AGPATs capable of catalysing the esterification of an activated FA (i.e acyl-CoA or acyl-ACP) onto LPA to make PA. We found two AGPAT candidates with conserved motifs: TGME49\_297640, and TGME49\_240860. Phylogenetic analyses reveal that TGME49\_297640 clusters with the prokaryotic clade of the pathway with plant and algal sequences and that TGME49\_240860 clusters with the eukaryotic clade of the pathway (**Figure S1**). So we termed these enzymes *TgATS2*, and *TgAGPAT* based on the plant and eukaryotic terminology, respectively. We generated parasite lines expressing *TgATS2* and *TgAGPAT* endogenously tagged at the C-terminus with a triple HA tag, under control of their respective promoters (**Figures S2A-C**). Immunofluorescence assays (IFAs) confirmed *TgATS2* targets to the apicoplast (**Figure 1A**), and transient expression of *TgAGPAT*-HA showed a perinuclear structure corresponding to the parasite ER (**Figure 1B**).

To test if *TgATS2* and *TgAGPAT* have predicted 1-acylglycerol-3-phosphate acyltransferase activity, we complemented an *E. coli* temperature sensitive mutant

SM2-1  $\Delta pIsC$  lacking AGPAT activity (Coleman, 1990), with recombinant *TgATS2* and *TgAGPAT*. All transformants grew at the permissive temperature of 30°C (**Figure 1C**). Only those complemented with bacterial *EcPlsC* and *TgATS2* grew at the non-permissive 42°C (**Figure 1C**). Constructs with *TgAGPAT* including or not its long N-Ter extension, did not grow at 42°C likely because of *TgAGPAT* eukaryotic origin (**Figure S1**). Indeed, eukaryotic AGPATs favour acyl-CoA substrates over acyl-ACP substrates used in bacterial and plastid systems. Thus, it is unclear if *TgAGPAT* has acyltransferase activity, but *TgATS2* complements defective *E.coli* SM2-1 AGPAT enzymatic activity *in vivo*, confirming LPA to PA synthetic capability.

To investigate the importance of apicoplast *TgATS2* during tachyzoite life stages, the *TgATS2* locus was disrupted to generate knock-in (KI) and knock-out (KO) mutants of *TgATS2* using CRISPR-Cas9 strategies (**Figures S2D-F**). Loss of the protein product was confirmed by western blot (**Figures 1DE**), IFA (**Figure 1F**) and PCR (**Figures S2EF**). Both  $\Delta TgATS2$  mutants were viable but plaque and replication assays revealed that  $\Delta TgATS2$  had a mild yet significant growth defect with significantly more small (2-4 parasites) vacuoles, and significantly fewer large vacuoles (**Figures 1GHI**).

Parasite egress was significantly affected in the  $\Delta TgATS2$  mutant, (**Figure S2G**), but invasion ability showed no difference with the parental line, nor was there a defect in microneme secretion (**Figures S2HI**). Morphology of different intracellular tachyzoite organelles showed no obvious defects except the apicoplast displaying a mild biogenesis defect (**Figures S2JK**).

Upon closer inspection of parasite morphology,  $\Delta TgATS2$  parasites appeared fused to each other at their basal poles (**Figure 2A**), suggesting a cytokinesis defect, which provided a rationale for the egress defect (**Figure S2G**). Cytokinesis was monitored

173 by localizing MORN1, which curiously displayed no obvious mis-localization (**Figure**  
174 **2B**). However,  $\Delta TgATS2$  parasites showed important enlargement of the residual  
175 body (**Figure 2C**). Residual body size was quantified by IFA using GAP45 antibody  
176 as a marker for the inner membrane complex (IMC).  $\Delta TgATS2$  parasites displayed a  
177 significantly larger residual body at the centre of big vacuoles (>4 parasites),  
178 (**Figures 2BC**). Accordingly, egressed extracellular parasites often remained  
179 tethered at their basal pole via a plasma membrane (PM) structure (**Figure 2D**).  
180 Electron microscopy (EM) of  $\Delta TgATS2$  parasites supported the segregation defects  
181 seen by IFA (**Figure 2E**). In dividing parasites, it is commonly seen that the PM is  
182 kept connected between two recently divided cells so that the cells are stuck together  
183 and distributed to daughter cells during cytokinesis. Very little is known on the  
184 molecular mechanisms of PM segregation during cytokinesis. In the parental  
185 parasites, initial steps of endodyogeny showed the formation of the daughter cell  
186 apical pole along with organelle division before the formation of the daughter cells  
187 within the mother cell (**Figure 2E**). Emergence of the daughter cells initiates the  
188 apical-to-basal biogenesis of their PM, partly recycled from the mother (**Figures 2E<sup>1-</sup>**  
189 **5**), and ends by a constriction of both IMC and PM at the basal poles, leaving a small  
190 basal residual body (**Figure 2E<sup>6</sup>**). In contrast, there were many division and  
191 cytokinesis defects in  $\Delta TgATS2$ , which were unable to separate although a new  
192 round of daughter formation could be initiated (**Figure 2E<sup>1</sup>**). Furthermore, parasite  
193 organelles were frequently found in the residual body as if ejected from improper  
194 segregation likely contributing to the enlarged residual body phenotype (**Figure 2E**).  
195 Affected vacuoles thus displayed enlarged residual bodies that often contained  
196 various organelles—including the nucleus, mitochondrion, acidocalcisome vesicles,  
197 and other cytosolic material—that appeared to be ejected from the dividing cells due

to improper segregation (**Figures 2E<sup>3,4</sup>**). Pieces of mitochondria were a particular feature within enlarged residual bodies (**Figures 2E<sup>5,6</sup>**).

We attempted to disrupt *TgAGPAT* using CRISPR-Cas9 as per  $\Delta TgATS2$ , in wild type ( $\Delta TgAGPAT$ ) and  $\Delta TgATS2$  ( $\Delta TgAGPAT$ - $\Delta TgATS2$ ) genetic backgrounds but parasites were not viable (**Figures S2L-O**), suggesting *TgAGPAT* is indispensable, consistent with its phenotype score (Sidik et al., 2016).

***TgATS2* disruption reduces C14:0 FA incorporation into *T. gondii* lipids, skews the LPA/PA ratio, and alters phospholipid abundance and composition.**

To investigate the role of *TgATS2* in lipid metabolism, we performed lipidomic analysis on the  $\Delta TgATS2$  mutant. Disruption of *TgATS2* resulted in a large significant reduction of the relative amount of C14:0, main product of the apicoplast FASII (**Figures 3AB**). Significant decreases in C18:1 and C20:1 were also observed (**Figures 3AB**). In contrast, there was a significant increase in the abundance of C18:0, C22:1, C24:1, C20:4, C20:5 and C22:6 (**Figures 3A-C**), most of which can be scavenged from the host such as C20:4 and C20:5 (Welti et al., 2007, Ramakrishnan et al., 2012, Amiar et al., 2016)(**Figures S3AB**). Comparison of the relative FA abundance between  $\Delta TgATS2$  and its parental line showed significant decrease of C14:0, C20:0, C20:1 and C22:2 (**Figures 3C**). These results indicate that in addition to the aforementioned cytokinesis defect,  $\Delta TgATS2$  has a highly modified lipid content that relies more on long chain fatty acids scavenged from the host (**Figures 3A-C**).

To further investigate  $\Delta TgATS2$  lipid defects, we analysed and quantified each PL class and its individual FA content. The  $\Delta TgATS2$  mutant accumulates significantly more LPA compared to the control parental line and significantly less PA (**Figures 3DE**), consistent given that LPA and PA are the likely substrate and product of *ATS2*

223 respectively (**Figure 1C**). The slight reduction in PA suggests that *Tg*ATS2 is not  
224 responsible for the bulk PA synthesis but rather for a specialist function. Importantly,  
225 the LPA/PA ratio was significantly affected in  $\Delta TgATS2$  (**Figure 3E**). We investigated  
226 diacylglycerol (DAG) and other related PL, namely PC, PE, PI, PS,  
227 phosphatidylglycerol (PG) and cardiolipin (CL, **Figure 3D**). The relative abundance of  
228 both DAG and PG significantly decreased in  $\Delta TgATS2$  (**Figure 3D**). This is relevant  
229 since DAG can be a direct product of PA, and PG is the sole PL made from PA in  
230 plant chloroplasts (Ohlrogge and Browse, 1995). In contrast, the relative abundance  
231 of PS, PI and PE increased in the mutant (**Figure 3D**).

232 We then examined the FA profiles of each of these lipid classes. LPA had significant  
233 increases in the amounts of C16:0 and C18:0 in  $\Delta TgATS2$  parasites, whereas  
234 significant decreases in the apicoplast-specific FA, C12:0 and C14:0 were measured  
235 in the mutant (**Figure 3F**). No major difference was observed in PA composition in  
236  $\Delta TgATS2$  parasites (**Figure 3G**). Strikingly though, DAG, PC, PI and PE all had  
237 significantly reduced C14:0 content (**Figures 3D, S3C-H**), which is the main product  
238 of FASII, and is used by *Tg*ATS1 for bulk *de novo* synthesis of PC, PI and PE (Amiar  
239 et al., 2016). This indicates that *Tg*ATS2 likely uses apicoplast generated C14:0 as  
240 its major substrate to make these lipids. In contrast, the levels of two long,  
241 polyunsaturated FAs (PUFA), C20:4 and C20:5, in all three major PL (PC, PI and PE)  
242 were significantly increased in  $\Delta TgATS2$  (**Figure S3C-H**), which is again consistent  
243 with mutant parasites compensating for the lack of *de novo* made FAs by increasing  
244 scavenging long chain FAs from the host. The FA composition of foetal bovine serum  
245 (FBS) and HFF host cells (**Figure S3 C-H**) confirmed that C20:4 and C20:5 PUFA  
246 were present from the host environment. This is consistent with the  $\Delta TgATS2$   
247 mutants increasing scavenging of these PUFAs to make PC, PI and PE. We

complemented  $\Delta TgATS2$  and wild type parasites (**Figure S3I**), using exogenous PA(14:0;14:0), the putative product of *TgATS2*, and PA(16:0;18:1) as host derived PA. Proliferation assays showed that both exogenous PA sources could significantly boost parasite growth (**Figures S3IJ**), but could not rescue  $\Delta TgATS2$  growth phenotype. This indicates that the PA source needs to be made *de novo* via *TgATS2* for proper division. Since parasites are capable of scavenging lipids from the host and medium, we determined whether the  $\Delta TgATS2$  imported more PA, PC was used as a control.  $\Delta TgATS2$  imported significantly more PA and PC than the parental control line (**Figure S3K**). Together these data on extracellular  $\Delta TgATS2$  corroborate our lipidomic analyses (**Figure 3**) indicating that the mutant scavenges more lipids to compensate for reduced *de novo* synthesis.

#### **Disruption of *TgATS2* induces a mis-localisation of the parasite DrpC perturbing parasite cytokinesis, IMC formation and PM stability**

Lipidomic analyses revealed a drastic LPA/PA imbalance in the  $\Delta TgATS2$  mutant (**Figure 3E**). LPA and PA have important structural influences on membrane architecture and endocytosis by inducing local membrane curvatures, which can impact the recruitment and functions of specific dynamins at precise membrane domains for organelle/vesicle fission (Adachi et al., 2016, Schmidt et al., 1999, Gras et al., 2019). For example, synaptic vesicles transport between neurons requires a protein complex composed of a dynamin and an endophilin that exerts an acyltransferase activity to create the proper membrane groove where the dynamin can pinch and release the synaptic vesicle; or in human mitochondrial fission by the protein Dynamin-like 1, *HsDrp1*, which requires insertion, recruitment and regulation through PA. In *T. gondii*, there are three known Dynamin Related Proteins (Drps): *TgDrpA*, *TgDrpB*, and *TgDrpC*. *TgDrpA* and *TgDrpB* have roles in apicoplast fission,



and secretory organelle biogenesis, respectively (van Dooren et al., 2009, Breinich et al., 2009). *TgDrpC* was recently localized to the basal poles of dividing daughter cells (Heredero-Bermejo et al., 2019). We generated a parasite line expressing *TgDrpC* fused to a 3xHA tag under the control of its endogenous promoter using CrispR-Cas9 (**Figure S4AB**) and localized *TgDrpC*-HA during the tachyzoite intracellular division cycle in  $\Delta TgATS2$  and its parental line (**Figure 4A**). In parental line parasites *TgDrpC*-HA clustered in small punctate-like compartments in the apical post-Golgi area during interphase (**Figure 4A**). During daughter budding, *TgDrpC* re-localized to form two distinct ring-like structures coinciding with the growing ends of the IMC from the budding daughter cells, which constricted at the base of the mother cell during cytokinesis and eventually formed basal caps on the each newly divided parasite (**Figures 4AB**).

In  $\Delta TgATS2$ , localization of *TgDrpC*-HA was only mildly affected during interphase but was drastically affected during division (**Figures 4AB**). Indeed, *TgDrpC*-HA frequently failed to form the typical ring structures at daughter cells (**Figures 4AB**). Instead, DrpC-HA was scattered in the cytosol, or formed rings pushing on the side of mother IMC, or improperly constricted at the daughter basal pole (**Figures 4AB**). This contrasted with the normal localization of MORN1, which appears to be a more cytoskeletal component, as its localization remains unaffected during endodyogeny (**Figure 2B**). We further examined other known interactors of DrpC and thus localized the dynamin-like protein EPS15 (Heredero-Bermejo et al., 2019) by C-terminally tagging by CrispR-Cas9 (**Figures 4CD**). In parental strains, EPS15-HA localized to clear punctate dots during interphase similarly to DrpC. During endodyogeny, EPS15 remained as punctate dots and did not re-localize to the daughter rings like DrpC (**Figure 4C**). In  $\Delta TgATS2$  background, EPS15 was unaffected during interphase

though more scattered than in the parental line. However, during endodyogeny EPS15-HA mis-localized in the cytosol of the parasite when expressed in the  $\Delta TgATS2$  background (**Figure 4C**), consistent with its role as a DrpC interactor (Heredero-Bermejo et al., 2019).

*In silico* sequence alignment showed that (i) *TgDrpC* is the closest *TgDrp* homolog to the *HsDrp1*, which allows mitochondrial fission through its interaction with PA via its Stalk domain including a loop with specific hydrophobic residues (Adachi et al., 2016, Adachi et al., 2018); (ii) that the Stalk domain and the PA binding loop seem conserved in *TgDrC*; (iii) but are absent in *TgDrpA*, and *TgDrpB* (**Figures S4C-E**). To confirm this, we tagged and monitored the localization of other *TgDrps* in the  $\Delta TgATS2$  background. No obvious change in localization of *TgDrpA* was observed in  $\Delta TgATS2$  parasites, even during the fission of the apicoplast (**Figures S4B**).

Based on homology with *HsDrp1*, we disrupted the putative PA binding region of *TgDrpC*. We expressed this *TgDrpC*- $\Delta$ PA version of the protein in the parasite to test the importance of the putative PA binding domain for the localisation of *TgDrpC*. To do so, we transfected a Wild Type *TgDrpC*-HA cell line with a Cas9-RFP and a PCR product targeting the DrpC PA domain. IFAs on parasites with no Cas9-RFP had typical DrpC-HA localisation (**Figure 4D**). However, parasites with positive Cas9-RFP expression showed that DrpC was mis-localized and scattered throughout the cytosol in a similar manner as in *Tg $\Delta$ ATS2* parasites. These results are also consistent with the cytosolic mis-localisation of truncated *TgDrpC* excluding the putative PA binding domain recently reported (Melatti et al., 2019).

Further detailed evidence of improper cytokinesis could be observed under electron microscopy. In the parental line, initial steps of endodyogeny showed the formation of the daughter cell apical pole along with organelle division before the formation of the

daughter cells within the mother cell (**Figure 4E**). Emergence of the daughter cells initiates the apical-to-basal biogenesis of their PM, partly recycled from the mother (**Figures 4E<sup>1-5</sup>**), and ends by a constriction of both IMC and PM at the basal poles, leaving a small basal residual body (**Figure 3F<sup>6</sup>**). IMC biogenesis and aberrant endocytosis can be seen in *TgΔATS2* cells upon closer inspection under electron microscopy. In contrast  $\Delta TgATS2$  were unable to separate although a new round of daughter formation could be initiated (**Figure 4F<sup>1</sup>**). Daughter cells were found tightly apposed at normal emergence sites and their PMs were often missing between daughter IMCs. Instead, interconnection of PM, vesicles or cisternae could be observed at these apposition sites and at the basal end of dividing cells (**Figures 4F<sup>1,2</sup>**). Mother cells were frequently observed to be fused to each other with vesicle fusion frequently occurring between the two at the site of the PM (**Figure 4F<sup>2</sup>**). These defects suggested issues at the PM composition and/or problems in membrane fusion/fission sites. Furthermore, there was no constriction of both IMC and PM from daughter cells resulting in enlarged residual bodies containing organelles and cytosol portions (**Figures 4F<sup>3,4</sup>**). Particularly, these membrane invaginations were frequently seen at the junction between two parasites in a process resembling endocytosis.

**Nutrient starvation enhances the synthesis of FA by apicoplast FASII in *T. gondii* and blocks intracellular proliferation of *P. falciparum* blood stages lacking a functional FASII.**

Since *TgATS2* has a role in maintaining parasite lipid homeostasis, we set out to determine the balance of *de novo* synthesized versus scavenged lipids in  $\Delta TgATS2$  using a stable isotope precursor of apicoplast synthesised fatty acids, U-<sup>13</sup>C-glucose. (Ramakrishnan et al., 2012, Amiar et al., 2016, Dubois et al., 2018). Incorporation of <sup>13</sup>C within FA is detected by increase of mass and determined in relation to non-

labelled FA. Distribution of  $^{13}\text{C}$  incorporation to each FA isotopologue is shown as its own mass (M) plus number of  $^{13}\text{C}$  carbon incorporation, *i.e.* M+x. In both parental and  $\Delta TgATS2$  mutant lines, we observed significant differences of  $^{13}\text{C}$  incorporation in C14:0, C16:1, C18:0 and C18:1 (**Figure 5A**). Isotopologue distribution of apicoplast-signature C14:0 showed that  $\Delta TgATS2$  had  $^{13}\text{C}$  incorporation up to M+14 but major incorporation occurred at lower masses (M+8, M+10) than the parental (M+12, M+14, **Figure 5B**). This indicates that FASII is active in  $\Delta TgATS2$ , yet slowed down in the process of making C14:0, thus explaining the C14:0 reduction previously detected (**Figure 3A**). Similar significant results were observed for C16:0 isotopologue distribution although overall incorporation was similar between parental and  $\Delta TgATS2$  (**Figure 5C**). C18:0 in  $\Delta TgATS2$  had higher  $^{13}\text{C}$  incorporation than the parental and its isotopologue distribution showed more short FA from the apicoplast (**Figure 5D**).

Lipidomic analyses thus indicate that both scavenged and *de novo* lipid fluxes are modified in  $\Delta TgATS2$ . To tease out the impact of host nutritional environment on both pathways, we sought to measure parasite lipid fluxes under adverse host nutritional/lipid conditions, through limitations in FBS concentrations in parasite culture media. Interestingly, GC-MS analysis revealed that  $^{13}\text{C}$  incorporation into all FASII-generated and further ER-elongated FA products, *i.e.* C14:0, C16:0, C16:1, C18:0, C18:1, C20:1, was significantly higher by 5-15% under FBS starvation in the parental line (**Figures 5EF, S5A**). In addition,  $^{13}\text{C}$  incorporation into most FAs is increased in the wild type parental line (**Figure 5F**). These results suggest that apicoplast *de novo* FA/lipid synthesis can be upregulated during FBS starvation to compensate for the lack of nutrients in the external environment. However, in  $\Delta TgATS2$ , the  $^{13}\text{C}$  incorporation into each FA was decreased by FBS starvation

(**Figure 5F**). No morphological changes could be observed by IFA in the FBS starved WT or  $\Delta TgATS2$  mutant (**Figure S5B**). Both parental line and  $\Delta TgATS2$  mutant showed a significant reduction in the synthesis of C18:0 in FBS starved conditions, suggesting that C18:0 is predominantly obtained by scavenging from the host cell (**Figure 5F**). Since availability of lipids from the environment is limited, the FA abundance in the parental line was decreased (**Figure 5G**). Interestingly however, the FA abundance in  $\Delta TgATS2$  was increased in most of its FA species during FBS starvation (**Figure 5G**).

Although we observed a defect in the activation of FASII in  $\Delta TgATS2$ , FASII was nevertheless viable during FBS starvation. This suggests that if FASII is active, regardless of the level of FASII activity, the parasites are viable under FBS starvation, consistent with its essential role in tachyzoites. However, in *P. falciparum*, FASII is not essential during nutrient replete blood stage but is activated under lipid starvation, apparently to compensate for reduced availability of scavenge-able lipids (Yu et al., 2008, Botte et al., 2013). Our results in *T. gondii* led us to re-think the current hypothesis regarding the dispensability of the apicoplast FASII in *P. falciparum* blood stages and to test the essentiality of malaria parasite apicoplast FASII under nutrient/lipid starved conditions. We grew *P. falciparum* FASII KO,  $\Delta PfFabI$  (Yu et al., 2008) and its parental line (NF54) in either regular (i.e. lipid rich) culture medium or in “lipid-starved” minimal medium (Mi-Ichi et al., 2007, Botte et al., 2013). Both NF54 and  $\Delta PfFabI$  grew normally in the regular culture medium (**Figure 5H**). In the lipid-starved medium, NF54 was viable but grew significantly slower than in lipid replete conditions, as previously reported (Shears et al., 2017). However,  $\Delta PfFabI$  grew only for the first 2 days in lipid starved media, but after 4 days, a sharp decrease in growth occurred, and this led to a complete loss of detectable parasites

after 8 days and showed no sign of further recovery in the next monitored cycles  
(**Figure 5H**). This shows that FASII is required for the malaria parasite blood stages  
to adapt its lipid metabolism in response to an adverse host lipid environment, a  
similar situation to that revealed here for *T. gondii*.

Since environmental FBS starvation induces an increase of *de novo* lipid synthesis,  
we investigated the effect the lipid-nutrient depleted conditions (i.e. 0, 1, 10% of FBS)  
on various mutants involved in lipid metabolism in *T. gondii*. We assessed parasite  
growth by plaque assay and quantified plaque area. The wild-type and parental  
parasite lines could grow equally well in DMEM supplemented with 0, 1, or 10% FBS  
(**Figures 5I-R, S5C**), without affecting the integrity of HFF host cells. FBS starvation  
reduced growth of  $\Delta TgATS2$  under 0% FBS (**Figure 5I**). *TgATS1* depleted cells grew  
sharply less in the regular culture conditions (i.e. 1% FBS), but starvation under 0%  
FBS led to the quasi-absence of plaques whereas an increase to 10% FBS partially  
rescued the growth defect seen in 1%FBS (**Figure 5J**). This suggested that in the  
absence of the major *de novo* PL precursor synthesis pathway, the parasite could  
partially compensate the growth defect by accessing more host lipid resources. The  
acetyl-CoA synthetase, *TgACS* (Dubois et al., 2018), was adequately responsive to  
FBS starvation (**Figure 5K**). Interestingly, proteins not involved in bulk  
membrane/lipid synthesis, such as *TgPKA-iKO*, could not be rescued by excess  
nutrients (**Figure 5L**) (Uboldi et al., 2015).

Since host fatty acid binding proteins (FABP) are upregulated upon tachyzoite  
invasion (Hu et al., 2017), we searched the genome of *T. gondii* for homologs of  
FABP that could be responsible for the transport of FAs in the parasite during  
starvation but found none. Instead, we found two proteins belonging to the closely  
related family of acyl-CoA binding protein (ACBP), i.e. *TgACBP1* and *TgACBP2*. We

identified that *TgACBP1* and *TgACBP2* localised at the parasite cytosol and mitochondrion, respectively (**Figures S5D-G**). We generated inducible knock-down parasite lines for both (**Figures S5DE**). However, plaque assays showed that both proteins were dispensable during tachyzoite life stages and neither were responding to FBS starvation (**Figures 5MN**), suggesting that neither of the *TgACBPs* are involved as effectors for the adaptation to nutritional environment. We generated a *TgACBP1* and *TgACBP2* double KO, and a double *ACBP1iKD*/Sterol Carrier Protein (SCP2) KO cell line, which we also found to be viable and not responsive to starvation (**Figures S5HI**).

We then hypothesized that parasite effectors putatively exported into the PVM or towards the host cell could be used by the parasite to collect putative host membrane material generated during FBS starvation. To test this, we investigated *TgASP5*, a Golgi-resident aspartyl protease that controls the non-canonical trafficking pathway of parasite effectors towards the PVM and the host cell, during FBS starvation (Bougdour et al., 2014). Strikingly, FBS starvation significantly exacerbated the growth defect in  $\Delta TgASP5$  (**Figures 5O, S7**). By contrast, the mutant cell line  $\Delta TgMYR1$ , (the canonical system to export effectors towards the host (Franco et al., 2016), showed overall less growth than the parental cell line, although  $\Delta TgMYR1$  grew equally well between the 0, 1, 10% FBS conditions (**Figure 5P**). To examine the effects of some specific GRA effectors, we examined a GRA16 KO cell line, which we observed to have a minor but significant growth defect under FBS starvation suggesting that at least some GRA proteins are important likely in combination (**Figure 5O**). We also examined a mutant for rhoptry secretion *TgARO-iKO* (Mueller et al., 2013) but found that under ATc treatment the mutant died regardless of FBS

concentration (**Figure 5R**) suggesting a primary role in host invasion prior to host re-wiring.

Lastly, we explored strain specific differences between in *Toxoplasma* between the hypervirulent Type I RH strain, and Type II strains (Prugniaud, ME49) capable of forming chronic stages (bradyzoites). Both Type II strains showed significantly reduced growth in lipid-depleted medium (**Figures 5ST**) unlike Type I strain.

Together, these data provide evidence that, in response to nutrient starvation, parasite effectors can be trafficked to the host cell primarily via the *TgASP5* export pathway likely to enhance the ability to scavenge resources.

#### **Nutrient starvation induces the formation of multi-membrane bound vesicles in host cells that are taken up by the parasite**

To investigate potential changes to the host cell and hence host/parasite interactions during lipid starvation we performed EM on starved (0, 1 or 10% FBS) HFF host cells infected with either the parental parasite line or  $\Delta TgATS2$ . Growth in 10% FBS led to no obvious phenotype changes in the hosts cells or the parental parasite line or the  $\Delta TgATS2$  mutant (**Figures 6AB**), but reduction to 1% and 0% FBS induced striking changes in the host cells, which became extensively vesiculated irrespective of whether they were infected with the parental line or  $\Delta TgATS2$  (**Figures 6AB**). Such vesiculation was not observed in uninfected HFF host cells put under nutrient starvation. Giant multi-vesicular bodies (gMVB), i.e. large membrane bound compartments containing various smaller vesicles, were frequent in 1% FBS grown cells (**Figures 6AB**) and very numerous at 0% FBS (**Figures 6AB**). The gMVBs are distinct from host autophagosome as they lack the typical double/multiple surrounding membranes and the cytosolic material defining autophagosomes (Ylä-



471 Anttila et al., 2009). This was confirmed by IFA using the typical autophagosome  
472 marker anti-LC3, which showed no accumulation of autophagosome under 10%, 1%  
473 or 0% (**Figure S8**). The gMVBs could arise from the host ER, as the ER could be  
474 seen swelling and forming networks containing large lipid bodies (**Figure 6B<sup>3</sup>**).  
475 gMVBs were also often seen in close apposition/contact with the mitochondria and/or  
476 ER network, indicating that material could also be transferred from both (**Figures**  
477 **6B<sup>3,5</sup>**). However, gMVBs were more often observed arising directly from the host  
478 nuclear envelope, potentially a major contributor for their formation (**Figures 6B<sup>6-8</sup>**).  
479 The gMVB accumulated in close vicinity with the PVM, which houses the parasite  
480 during its intracellular development and serves as the exchange interphase between  
481 the host and the parasite. The gMVBs were not only close to the PVM but appeared  
482 to be interacting with the PVM with host material and vesicles from the gMVB  
483 apparently “percolating” through the PVM (**Figure 6B<sup>4</sup>**) or directly from their  
484 originating organelles (**Figure 6B<sup>5</sup>**) to eventually be found in the PVM (**Figures**  
485 **6AB<sup>1</sup>**). These vesicles appeared in both wild-type and  $\Delta TgATS2$ , suggesting that the  
486 host cell is responding to the nutrient deficiency in the same way. The  $\Delta TgATS2$   
487 parasite cytokinesis phenotype (e.g. **Figure 2A**) was still observed and apparently  
488 exacerbated in 0% and 1% FBS growth medium (**Figure 6B**). This vesicle/gMVB  
489 formation and trafficking to and within the PVM was not apparent in high (10%) FBS  
490 medium, suggesting that host gMVBs somehow allow the parasite to increase its lipid  
491 scavenging in the absence of nutrient rich serum. Together this indicates that gMVB  
492 containing multiple vesicles, that (i) are dependent and induced by nutrient  
493 availability, and (ii) originate directly from diverse host organelles. The gMVBs are  
494 distinct from lipid droplets of host cell origin used as a lipid source by *T. gondii* (Nolan  
495 et al., 2017, Romano et al., 2017).

However, it is possible that FBS starvation leads to increased host cell lipid droplet import. Nile red staining confirmed that FBS starvation induced a significant increase of the amount of lipid droplets into the parasites and its PVM (**Figure 6C**). In contrast, low FBS content resulted in a reduced amount of lipid droplets in uninfected host cells whilst high FBS content increased their presence in the host cells alone (**Figure 6D**). This further indicates that increase of import of lipid droplets to the parasite is upregulated by the parasite during FBS starvation.

Since gMVB also seem to arise from host mitochondria, we used an anti-lyso-bi-phosphatidic acid (LBPA, i.e. a degradation product of mitochondrial cardiolipin) antibody (Kobayashi et al., 1998), lipid that can also be scavenged by intracellular parasites (Romano et al., 2017) (**Figure 6E**). LBPA was found surrounding the PVM in the host cell, within the PV and the parasite, but its localization and intensity remained unchanged in response to reduced FBS content (**Figure 6E**). Direct salvage of mitochondrial cardiolipin *per se* might not be the primary up-regulated scavenging pathway during lipid starvation.

To determine whether host mitochondrial sequestration could impact parasite adaptation to low host nutrient, we measured the levels of mitochondrial sequestration in Type I parasites (prone to host mitochondrial sequestration) and Type II parasites (not sequestering host mitochondria) (Pernas et al., 2014). Host mitochondria was monitored with mitotracker. Both RH Type I and Type II ME49 parasites showed no major difference in host mitochondrial sequestration after FBS starvation (**Figure S6**).

## Discussion

We have shown that *TgATS2* is an apicoplast acyltransferase able to esterify FAs on LPA to generate PA, a precursor for a wide range of parasite lipids. Knockout of

*Tg*ATS2 resulted in perturbed lipid fluxes, which impacts LPA/PA lipid balance causing mis-localization of *Tg*DrpC and vesiculation during cytokinesis. Furthermore, changes in lipid profiles of  $\Delta$ *Tg*ATS2 showed the capacity of wild-type parasites to exhibit considerable metabolic plasticity at both *de novo* FA synthesis in the apicoplast, and host modification for organelle membrane scavenging, together critical for adaptation to nutrient limiting conditions in the host (**Figure 7, Table S1**).

#### **PA and LPA roles in membrane curvature and cell division**

Membrane PLs have different physical shapes according to the relative sizes between the polar head and the fatty acid tails. Most PLs are cylindrical, while PA is cone shaped and LPA adopts an inverted cone shape, thus their insertion into membrane bilayers facilitates curvature and in/evagination (Kooijman et al., 2005).

Furthermore, in human cells, dynamin pinching requires endophilin1, an ATS2 homolog, as partner to create LPA/PA curvatures (Burger et al., 2000, Shin and Loewen, 2011). Improving penetration of a larger part of dynamin into the lipid monolayer (Burger et al., 2000, Shin and Loewen, 2011), similar to the relationship between *Tg*ATS2 and *Tg*DrpC. Our results reveal the previously unrecognised importance of the apicoplast in maintaining internal lipid homeostasis. Furthermore, the functional role of *Tg*ATS2 for PA synthesis during division provides a mechanism for the long-standing question of why drugs targeting the apicoplast display a secondary cytokinesis defect (Martins-Duarte et al. 2015).

Our results nicely complement a recent study, which identified the basal complex as a major site of endocytosis in motile tachyzoites, consistent with the basal complex localization of DrpC (**Figure 4**, (Heredero-Bermejo et al., 2019). Our results show that endocytosis occurs during intracellular stages and that aberrant LPA/PA ratios caused by the loss of ATS2 disrupts this process.

Furthermore, many DrpC interacting proteins have been identified as part of a larger endocytic protein complex, including EPS15, AP2 adaptins, and intriguingly, Kelch13 (Heredero-Bermejo et al., 2019). Kelch13 is the infamous protein found mutated in artemisinin resistant malaria spreading throughout Asia (Menard and Dondorp, 2017). Kelch13 therefore likely has a role in endocytosis consistent with DrpC and other interacting partners (Heredero-Bermejo et al., 2019). Intriguingly, It has been shown that FASII activity is often increased in artemisinin resistant parasites (Chen et al. 2014). Our evidence here demonstrates that the upregulation of FASII produces LPA that modulates cytokinesis and endocytosis processes. Again, this highlights the previously unrecognised importance of the apicoplast in maintaining internal lipid homeostasis in parasites.

#### **Environmental and nutritional conditions drive the adaptation of the apicoplast metabolic capacities as well as the scavenging capacities**

Importantly, *Toxoplasma* could increase production of FA in the FASII pathway in nutrient/lipid deprived medium similarly to *P. falciparum* (Botte et al., 2013). Hence, apicomplexan parasites show high metabolic flexibility to obtain FA for the major membrane building blocks required for growth as pointed out by recent studies exploring *Plasmodium* survival in nutrient depleted conditions (Mancio-Silva et al., 2017, Zuzarte-Luis et al., 2017). Importantly, our results demonstrate that *P. falciparum* lacking a FASII and grown in lipid-deprived conditions, were unable to properly proliferate, ultimately dying. This suggests that apicoplast FASII is facultative rather than totally dispensable in malaria parasite blood stage and can be activated during lipid starvation to meet PL needs. This FASII flexibility is consistent with a growing pool of evidence including the upregulation of FASII and the apicoplast acyltransferase PfG3apiGPAt (homolog of *TgATS1*) transcripts in starved patients

(Daily et al., 2007) and the essentiality of most FASII enzymes including the central acyl-carrier protein, ACP in both *T. gondii* and *P. falciparum* (Sidik et al., 2016, Zhang et al., 2018), summarized in **Table S1**. Therefore, environmental factors could have important consequences in treating patients. Indeed, if patients are under stress/nutrient deprivation/malnourished conditions, then the FASII pathway could become a secondary target of choice to help eradicate the parasites. Altogether this data questions whether isopentenyl pyrophosphate (IPP) synthesis is the sole essential function of the apicoplast during *Plasmodium* blood stage (Yeh and DeRisi, 2011). Rather our data puts the parasite back into its physiological context where nutrient availability and environmental conditions drive the requirement and regulation of a given metabolic pathway. Furthermore, the scavenging of *Toxoplasma* can also be seen to be upregulated through exported effectors by evidence that the ASP5 KO is partially rescued by excess host lipids and the induction of host remodelling to make gMVBs, although the identity of these gMVBs warrants further investigation. This redefines what we call an essential gene, where phenotypes might only be seen under starvation conditions.

A major question raised here is the nature the signalling factor(s) responsible for environmental sensing and metabolic adaption of both apicoplast *de novo* synthesis and scavenging pathways. Both *T. gondii* and *P. falciparum* lack the canonical mTOR-based nutrient-sensing pathways present in other eukaryotes but a recent study showed that *P. berghei* is capable of sensing nutrient deprivation by a SNF1-related kinase, KIN1 (Mancio-Silva et al., 2017).

Together, our results reveal the central role of the apicoplast to provide specific precursors for membrane biogenesis during cytokinesis and most importantly to be a central metabolic hub to adapt the parasite metabolic capacities upon nutrient

availability and environmental changes. The data also point at major modifications in vesiculation and utilization/scavenging of these membrane structures by the parasite upon such environmental changes. Data also corroborate recent results with the mosquito lipid environment regulates the metabolic activity of transmissible sporozoites (Costa et al., 2018). The fundamental role of these physiological changes induced by the parasite in response to host environment provides novel insights in the parasite biology and offers new avenues to explore in the fight against toxoplasmosis and malaria.

**Acknowledgement:** We would like to thank Prof Alan Cowman, and Dr Ali Hakimi for sharing parasite strains, reagents, and fruitful advices. This work and CYB, YYB, SA, NJK, CB are supported by Agence Nationale de la Recherche, France (Grant ANR-12-PDOC-0028- Project Apicolipid), the Atip-Avenir and Finovi programs (CNRS-INSERM-FinoviAtip-AvenirApicolipid projects), and the Laboratoire d' Excellence Parafrap, France (grant number ANR-11-LABX-0024). CYB and GIM are supported by the LIA-IRP CNRS Program (Apicolipid project).

**Author contributions:**

SA and NJK designed and performed experiments, analysed and interpreted data, and wrote the manuscript. LB performed, analyzed and interpreted data for electron microscopy. SD performed Nile Red/LBPA and related IFAs. SD generated and analysed the *TgDrpC-ΔPA* mutant. CSA generated and analysed the double ACBP1-ACBP2 and ACBP1iKD/SCP2KO mutants. MJS helped performing and analysing the *P. falciparum* lipid starvation growth assay. CB helped performing *E. coli* complementation assays. BT performed and analysed *T. gondii* proliferation assays and the related statistical analyses. GIM supervised the *P. falciparum* lipid starvation growth assay. YYB performed, analysed interpreted and supervised lipidomic

621 analyses data and wrote the manuscript. CYB lead the project, designed and  
622 interpreted data and wrote the manuscript.

623 **Declaration of interest:** Authors declare no conflict of interest.

624

## Figures legends

**Figure 1: *Tg*ATS2 is an apicoplast lysophosphatidic acid acyltransferase important for parasite proliferation. (A, B)** IFA of stable *Tg*ATS2-HA expressing parasites **(A)** and transient *Tg*AGPAT-HA expression **(B)**. CPN60: apicoplast marker; TOM40, mitochondrial marker. Scale bars=2  $\mu$ m **(C) Expression of *Tg*ATS2 and *Tg*AGPAT in LPAAT deficient *E. coli* strain SM2-1** SM2-1 $\Delta$ p/sC *E. coli* mutant transformed with *Tg*ATS2 (1, 2), *Tg*AGPAT (1, 2), *Tg*AGPAT $_{\Delta$ Nter1-72}, *Ec*plsC or empty pQE30Xa expression vector were grown at 30°C (permissive) or 42°C (non permissive) for 20 h (n=3). **(D, E)** Confirmation of *Tg*ATS2-HA loss by Western blot analysis in *Tg*ATS2-KI **(D)** and *Tg*ATS2-KO **(E)** using anti-HA (anti-Gra1: loading control). **(F)** Confirmation of *Tg*ATS2-HA-signal loss in  $\Delta$ *Tg*ATS2 by IFA using anti-HA (Scale bars=2  $\mu$ m). **(G)** Plaque assay showing a mild growth defect in  $\Delta$ *Tg*ATS2 mutants **(H)** Cell-based growth fitness assay confirmed the growth defect in the  $\Delta$ *Tg*ATS2 mutants 30 h post-infection (n=3). **(I)** Proliferation assay confirmed a replication defect in  $\Delta$ *Tg*ATS2 mutants (n=3). \*, p  $\leq$  0.05; \*\*, p  $\leq$  0.01; \*\*\*, p  $\leq$  0.001; \*\*\*\*, p  $\leq$  0.0001.

**Figure 2: Disruption of *Tg*ATS2 induces parasite cytokinesis defect, residual body enlargement and organelle segregation deficiency. (A)** IFA of  $\Delta$ *Tg*ATS2-HA and parental line using anti-HA and anti-IMC1 shows that  $\Delta$ *Tg*ATS2-HA has a cytokinesis defect phenotype (scale bars=2  $\mu$ m) **(B)** IFA of  $\Delta$ *Tg*ATS2 and parental line transiently expressing MORN1-mCherry (IMC basal tip) and anti-IMC1 (scale bars=2  $\mu$ m). Confirmation of enlarged residual bodies in  $\Delta$ *Tg*ATS2 by IFA using anti-GAP45 (IMC marker) **(C)**, and by statistical analysis of residual body size **(D)**. **(E)** IFA observation of extracellular parasites using anti-SAG1 reveals egressed parasites tethered at their basal ends (white arrowhead: PM tether). **(E)** Electron microscopy



650 image of  $\Delta TgATS2$  mutants reveals important cytokinesis defects: major enlargement  
651 of the PM, defects in mother cell membrane constriction and cell daughter  
652 attachment at the basal pole (**1, 2, enlarged in 1', 1'', 2'**, white arrows), IMC  
653 fragmentation at the separation sites between dividing parasites (**2''**). Residual  
654 bodies containing unevenly separated nuclei (**1, 3, 3', 4, 5**), mitochondria (**4, 5, 6, 6'**)  
655 and acidocalcisomes (**5**). **N**: nucleus; **Mt**: mitochondria; **rb**: residual body; **Ac**:  
656 acidocalcisome (scale bars= 1  $\mu$ m).

657 **Figure 3: Lipidomic analysis  $\Delta TgATS2$  mutant. (A, B)** Fatty acid composition of  
658 total lipid extracted after 72 h post-infection **(C)** Relative fatty acid abundance of  
659  $\Delta TgATS2$  to the parental line. **(D)** Relative major phospholipid abundance of  
660  $\Delta TgATS2$  to parental line **(E)** LPA/PA ratio. Individual molecular species of LPA **(F)**,  
661 PA **(G)**, DAG **(H)**. Fatty acids are shown as Cx:y as x for number of carbons and y for  
662 the number of unsaturations. n=4, \*,  $p \leq 0.05$ ; \*\*,  $p \leq 0.01$ ; \*\*\*,  $p \leq 0.001$ ; \*\*\*\*,  $p \leq 0.0001$ .

663 **Figure 4:  $\Delta TgATS2$  induces the specific mislocalization of *TgDrpC*, a dynamin-**  
664 **related protein involved in endodyogeny, that leads to cytokinesis defects**  
665 **during tachyzoite division.**

666 **(A)** IFA localization of *TgDrpC*-HA expressed in parental line shows ring structures at  
667 the growing ends of daughter cells during division (top panel) but fails to do so when  
668 expressed in  $\Delta TgATS2$  (bottom panel). **(B)** *TgDrpC*-HA localisation during tachyzoite  
669 division cycle in the parental line (top panel) and its mislocalization in  $\Delta TgATS2$   
670 mutant. Scale bars= 2  $\mu$ m. **(C)** IFA localization of TgESP15, a known interactor of  
671 *TgDrpC*, in  $\Delta TgATS2$  and parental line using anti-HA and anti-IMC1. Scale bars= 2  
672  $\mu$ m. **(D)** IFA localization of *TgDrpC* and *TgDrpC*- $\Delta$ PA domain-Cas9-RFP using anti-  
673 HA and anti-IMC1 (scale bars 2  $\mu$ m) reveals the mislocalization of *TgDrpC* $\Delta$ PA  
674 domain during endodyogeny. **(E, F) Electron microscopy** observation of

675 endodyogenic division in parental line **(E)** and  $\Delta TgATS2$  **(F)**. **(E<sup>1-3</sup>)** Endodyogeny  
 676 starts with the formation of daughter cells (dc) by growth of IMC (white arrows) and  
 677 organelles segregation. IMC scaffolding then grows towards the basal pole (white  
 678 arrows) encompassing divided organelles (eg nucleus N). **(E<sup>4-5</sup>)** Recycling and  
 679 biogenesis of PM (black arrow) ends daughter cell emergence from mother cell (mc).  
 680 **(E<sup>6-6</sup>)** Division ends by cytokinesis through constriction of both IMC and PM at basal  
 681 pole (black arrows) to form a small residual body (rb). **(F)**  $\Delta TgATS2$  shows an  
 682 incomplete separation of daughter cells during cytokinesis with absence of PM  
 683 biogenesis between closely apposed IMC **(F<sup>1,3</sup> and insets, white arrows)**, presence  
 684 of vesicle/cisternae inside membrane structures at the inter-IMC space **(2' white**  
 685 **arrows)**, absence of mother IMC **(F<sup>3</sup> black arrow)**, absence of basal constriction  
 686 forming large residual bodies leaving floating daughter IMC **(F<sup>3,4, 4'</sup> white. arrows)**.  
 687 Scale bar = 1 $\mu$ m. **(G,H)** Proposed molecular model for *TgDrpC* function during  
 688 endodyogeny and cytokinesis in WT parasite **(G)** and  $\Delta TgATS2$  **(H)** LPA and PA  
 689 molecules induce positive and negative curvature creating grooves in membranes for  
 690 *TgDrpC* to insert at specific sites during division for a pinching function during  
 691 endodyogeny **(G)**

692 **Figure 5: Changes in host nutritional environment induces an upregulation of**  
 693 **the apicoplast FASII metabolic capacities in *T. gondii* tachyzoites and *P.***  
 694 ***falciparum* blood stages and is pivotal for enzymes involved in metabolic**  
 695 **adaptation. (A-G) U-<sup>13</sup>C-glucose labelling for 72 h to monitor apicoplast FA synthesis**  
 696 **by <sup>13</sup>C incorporation to fatty acids (Blue, parental line, Red,  $\Delta TgATS2$ ) (A) <sup>13</sup>C**  
 697 **incorporation to each fatty acids in 1% FBS (B-D) Mass isotopologue distribution in**  
 698 **1% FBS for C14:0 (B), C16:0 (C) and C18:0 (D) The x-axis shown as 'M+X'**  
 699 **represents mass with 'X' <sup>13</sup>C atoms incorporated during the FA synthesis. (E) <sup>13</sup>C**

700 incorporation to each fatty acids in 0.2% FBS. FASII metabolic activity increased  
 701 upon FBS starvation in the parental line but not in  $\Delta TgATS2$ . **(F)** Change in the  $^{13}C$   
 702 incorporation between 0.2%FBS and 1% FBS (-FBS/+FBS) **(G)** The relative  
 703 abundance of each FA (-FBS/+FBS) **(H)** Asexual blood stage growth assay of *P.*  
 704 *falciparum* FabI-KO and its parental line (NF54) in regular (lipid rich) culture medium  
 705 and lipid starved medium reveals that FASII is essential in blood stage in low-lipid  
 706 environment. **(I-T)** Growth assays conducted in 0, 1, or 10% FBS in different *T. gondii*  
 707 mutants and strains; *TgATS2* **(I)**, *TgATS1* **(J)**, *TgACS* **(K)**, *TgPKA* **(L)**, *TgACBP1* **(M)**,  
 708 *TgACBP2* **(N)**, *TgASP5* **(O)**, *TgMyr1* **(P)**, *TgGRA16* **(Q)**, *TgARO1* **(R)** , Type II PRU  
 709 **(S)**, Type II ME49 **(T)**. n=3, or more. *p values*: ns, not significant, \*,  $p \leq 0.05$ ; \*\*,  $p \leq 0.01$ ;  
 710 \*\*\*,  $p \leq 0.001$ ; \*\*\*\*,  $p \leq 0.0001$ .

711 **Figure 6: Nutrient starvation unveils formation of multi vesicular bodies from**  
 712 **host cell organelles, which content is imported towards parasites.** Transmission  
 713 electron micrographs of intracellular WT tachyzoites **(A)** and  $\Delta TgATS2$  mutant  
 714 parasites **(B)** grown in 0, 1 and 10% FBS. Nutrient starvation (i.e. 0 and 1% FBS)  
 715 induce formation of giant multivesicular bodies (gMVB) in the host cell (hc),  
 716 containing various vesicles including lipid bodies-like (white stars). In starvation,  
 717 gMVB localized in the cytosol (cyt) in contact to the parasitophorous vacuole (pv)  
 718 **(A<sup>1,2</sup>, B<sup>1,2</sup>)**, and their content was imported through and into the PV **(A<sup>1</sup> black stars,**  
 719 **B<sup>2,6</sup> black arrows)**, gMVB were arising from host endoplasmic reticulum (ER, **A<sup>2</sup>**),  
 720 mitochondria (mt, **A<sup>2,3</sup>**) and mainly swollen nuclear envelope (N, **B<sup>3,4,5</sup>**). 10% FBS did  
 721 not induce gMVB formation in both parental and  $\Delta TgATS2$ . Scale bar= 1 $\mu$ m. **(C)**  
 722 Nutrient starvation induces a significant increase of lipid droplets within the parasite  
 723 and its PV as measured by IFA using Nile red (Nile Red dots were counted for 100 or  
 724 more parasites n=3, *p values*: ns, not significant, \*,  $p \leq 0.05$ ; \*\*,  $p \leq 0.01$ ; \*\*\*,  $p \leq 0.001$ ;

725 \*\*\*\*,  $p \leq 0.0001$ ). **(D)** Nutrient starvation induces a decrease of lipid bodies in  
726 uninfected HFF host cells as measured by IFA using Nile red. **(E)** IFA shows that  
727 import into parasites of LBPA (anti-LBPA) is not affected by nutrient starvation. **(F)**  
728 Nutrient starvation induces a significant growth defect in *T. gondii* tachyzoites ME49  
729 Type II strain compared to RH Type I strain.

730 **Figure 7: Proposed model for cytokinesis, lipid acquisition and metabolic**  
731 **adaptation under adverse host lipid environment in *T. gondii*.** Under lipid rich  
732 environment, *T. gondii* can readily acquire FA and lipids by *de novo* synthesis  
733 (apicoplast) and host cell scavenging. The apicoplast ATS2 generates PA and  
734 regulates the balance of LPA/PA, necessary for DrpC. In a host lipid starved  
735 environment, the parasite adapts its metabolism by increasing FASII to produce more  
736 fatty acids to compensate their absence from the host cell. Concomitantly, the  
737 parasite induces morphological changes in the host to increase scavenged  
738 resources, including the nucleus, ER and gMVBs.

## **Materials and Methods:**

### **dKEY RESOURCES TABLE**

See STAR methods **KEY RESOURCES** Table

### **d LEAD CONTACT AND MATERIALS AVAILABILITY**

Materials generated in this study are available upon request. Information and requests for resources and reagents should be directed to the Lead Contact, Cyrille Botte (cyrille.botte@univ-grenoble-alpes.fr). Plasmids and parasite lines generated in this study will be made freely available by the Lead Contact upon request which may require the completion of a Material Transfer Agreement.

### **d EXPERIMENTAL MODEL AND SUBJECT DETAILS**

#### ***T. gondii* culture**

*Toxoplasma gondii* parental lines RH TATi1-ΔKu80 (Sheiner et al., 2011) and RH-ΔKu80 (Huynh and Carruthers, 2009) and derived transgenic cell lines were grown in confluent human foreskin fibroblasts (HFFs) in high glucose DMEM supplemented with 1% Foetal Bovine Serum, as described (Amiar et al., 2016). ME49 parental cell cultures were additionally supplemented with 10 mM HEPES.

#### ***P. falciparum* culture**

*P. falciparum* NF54 wild type parasites were maintained as previously described (Trager and Jensen, 1976). Briefly, *Plasmodium* blood stage parasites were maintained at 2% haematocrit in 1640 RPMI-HEPES supplemented with 10% AlbuMAX II (Gibco) and 0.25% gentamycin. Parasites were grown sealed Perspex chambers gassed with beta mix gas (1%O<sub>2</sub> 5%CO<sub>2</sub>, 94% N<sub>2</sub>) at 37°C and maintained on 48-hour cycles.

### **d METHOD DETAILS**

771 Gene identification and sequence analysis

772 *T. gondii* plasmid constructs

773 *T. gondii* transfection

774 *T. gondii* growth assays

775 *T. gondii* Red/Green parasite invasion assay:

776 *Plasmodium falciparum* growth assays:

777 Immunofluorescence assay and Microscopy

778 Nile red staining of lipid droplets

779 Activity analysis in LPAAT-deficient *E. coli* strains

780 Transmission electron microscopy:

781 Lipidomic analysis by GCMS extraction from *T. gondii* tachyzoites

782 Stable isotope labelling of *T. gondii*

783 Phospholipid import assay:

784 Quantification and statistical analysis

785

## Gene identification and sequence analysis

Arabidopsis thaliana sequence of ATS2 (GenBank<sup>TM</sup> and TAIR<sup>TM</sup> IDs: NP\_194787 and AT4G30580 respectively) was used as a query sequences for BLAST searches against the Toxoplasma gondii genome on ToxoDB database ([www.toxodb.org](http://www.toxodb.org)). Phylogenetic analysis of AGPAT related proteins was performed on the Phylogeny.fr platform (Dereeper et al., 2008). Protein sequences were then aligned by ClustalW software (Larkin et al., 2007) and the maximum likelihood phylogeny was generated using the PhyML (Guindon et al., 2010). We generated multiple sequence alignment using Clustal Omega (Li et al., 2015).

## *T. gondii* plasmid constructs

Plasmid LIC-3HA-DHFR was used to generate a 3' endogenous tagging with 3xHA coding sequence of TGME49\_297640 (*TgATS2*) and TGME49\_240860 (*TgAGPAT*). A 2229 bp fragment corresponding to the 3' of *TgATS2* was amplified from genomic DNA using primer sets 5'-TCCTCCACTTCCAATTTTAGCGTTCGTCTCGGTGGCGGC-3' and 5'-TACTTCCAATCCAATGCTTCAGACACTCGGTGCAAA-3. A 5466 bp fragment corresponding to promoter and gene sequence of *TgAGPAT* was amplified using primer sets 5'-TACTTCCAATCCAATGCAGCCAGCAAAGGACGAAAGG-3' and 5'-TCCTCCACTTCCAATTTTAGCGAGACCGTGGCCTCGGTGGG-3'. These fragments were cloned into pLIC-3HA-DHFR vector as described previously (Huynh and Carruthers, 2009). Vectors LIC-*TgATS2*-3HA-DHFR and LIC-*TgAGPAT*-3HA-DHFR were confirmed by PCR screen using primer sets 5'-GCATAATCGGGCACATCATA-3' and 5'-ATACGCATAATCGGGCACATCATA-3' and by sequencing (Eurofin genomics<sup>TM</sup>).

Plasmid pTOXO\_Cas9-CRISPR (gift from Hakimi Lab, Grenoble, France) was used to integrate a gRNA within BsaI restriction site as previously described (Sidik et al., 2014). Briefly, Crisp-Fwd and Crisp-Rv primer sets were phosphorylated and annealed: *TgATS2-KI*: 5'-AAGTTACGGGTGTGCGCCGCCTTGCG-3' and 5'-AAAACGCAAGGCGGCGCACACCCGTA-3', *TgATS2-KO*: 5'-AAGTTGGAGCGCCGACGGGCGACTGG-3' and 5'-AAAACCAGTCGCCCCGTGCGCGCTCCA-3', *TgAGPAT-KO*: 5'-AAGTTCTCTGCCGAGTTCCAATCGCG-3' and 5'-AAAACGCGATTGGAACCTCGGCAGAGA-3'. The gRNAs were then ligated into pTOXO\_Cas9-CRISPR plasmid linearized with BsaI, yielding pTOXO\_Cas9-CRISPR::g*TgATS2-KI*, pTOXO\_Cas9-CRISPR::g*TgATS2-KO* and pTOXO\_Cas9-CRISPR::g*TgAGPAT-KO*, respectively.

For *TgATS2* knockout by CRISPR-Cas9, an appropriate HXGPRT cassette amplified by PCR from pMini (kind gift from the Hakimi laboratory) using those primer sets, *TgATS2-KI*: 5'-GAGGCCCTGCGTCTCCTCAAGCG-AAAGGCGCCGCCACAGTCGACGGGTGTGCGCC-GCCTCAGCACGAAACCT-TGCATTCAAACC-3' and 5'-GCTACTCCTTCTTCCCCTCTCG-CGTTGTGTGTCTCCCCGTGCGTTCTGCGTCGCCAGCAGTGTCAGTGTAGCCTGCCAGAACA-3'; *TgATS2-KO*: 5'-GACACACAACGCGAGAGGGGAAGAAGGAGTAGCTCTCG-TCGCCTTTCCAGAAGGTACTCCAGCACGAAACCTTGCATTCAAACC-3' and 5'-CTTCG-CTGCTCGTTCGTCTTCATGTGGGGAAGGAGCAGCACGAAACCTTG-CATTCAAACC-3'.

*DrpA* and *DrpC* were localized by CRISPR Cas9 strategy. Guides were inserted into Cas9 U6 universal plasmid (Sidik et al., 2014) by either standard ligation of annealed primers or Q5 mutagenesis. Cells were transfected together with PCR product encoding either HA3-CAT and *DrpC* homology flanks, for *DrpC* or GFP sequence without selection and *DrpA* homology flanks for *DrpA*.



838 For DrpC HA3 CAT CRISPR Cas9 tagging, DrpC was tagged at the 3' terminus by  
839 CRISPR Cas9 (Sidik et al., 2014). For DrpC, the protospacer gaatggggcttgaaactgtg  
840 was chosen and primers 5' AAGTTgaatggggcttgaaactgtgG 3' and 5'  
841 AAAACcacagtttcaagccccattcA 3' were annealed together and ligated into U6  
842 universal plasmid (Sidik et al., 2014). The HA3-CAT cassette was PCR amplified by  
843 primers with 50 bp homology flanks (FOR aggaagttccggctcggttccgtcaccgtt-  
844 gaatggggctAAAATTGGAAGTGGAGGACGGG and REV gttcttcccagtgctctggcga-  
845 agtggggccagcacaagccaGTTGTAAAACGACGGCCAGTG) and overhang  
846 corresponding to the 3' end of DrpC and in frame with HAx3. 50 µg of both plasmid  
847 and PCR product were transfected and placed under chloramphenicol selection (Kim  
848 et al., 1993). DrpC was also localized by pLIC-HA3-CAT using primers  
849 TACTTCCAATCCAATTTAGCgcacggtctgtgttctacg and  
850 TCCTCCACTTCCAATTTTAGCagccccattcaacggtg (Sheiner et al., 2011). For DrpA,  
851 the protospacer gatggaggagttgattcctg was inserted into the Universal Cas9 Plasmid  
852 using the NEB Q5 site directed mutagenesis Kit with the oligos 5'  
853 gatggaggagttgattcctgGTTTTAGAGCTAGAAATAGC 3' and 5'  
854 AACTTGACATCCCCATTTAC 3'. PCR product was amplified using 5'-  
855 gttgccctggcttctctcttctctctctctcaagATGGCGGTGAGCAAGGGC3' 5'-  
856 cgtcctgcaggcgattgacAacaggaatcaactctccatCCCGGGCTTGTACAGC 3' using GFP  
857 cDNA as a template and co-transfected with U6 guide RNA plasmid described above.  
858 Transfected parasites were seeded onto coverslips and then transiently observed  
859 after 24 hours growth.

860 For the DrpC PA domain mutation, a guide was identified within a DrpC exon and the  
861 20 bp protospacer (5' ggcgagctgacctcgaggt 3') was inserted into a CRISPR Cas9  
862 plasmid using Q5 with primers 5' ggcgagctgacctcgaggt-  
863 GTTTTAGAGCTAGAAATAGCAAG 3' and 5' AACTTGACATCCCCATTTAC 3'  
864 (Sidik et al. 2014). The PCR product was amplified with the following primers 5'  
865 cgtcgccttgtagcgaaacgctt-ggagacgcaaaaacggattGCGGTGAGCAAGGGCG 3' and 5'  
866 agccccattcaacggtgacggaagccgaccggaacttctgcCCCGGGCTTGTACAGC 3'. The  
867 guide and the PCR product were transfected together and parasites were seeded  
868 onto HFFs on coverslips and grown for 24 h. Cells were labelled with anti-IMC and  
869 anti-HA antibodies and viewed under the microscope. Cas9 expression was  
870 visualized by the Cas9-RFP tag to observe parasites with DrpC-HA normally (Cas9-  
871 RFP absent) or with the PA binding domain disrupted (Cas9-RFP present).

872 For TgACBP1i-HA KD, the 5' UTR flank was PCR amplified using primers  
873 ACACGGGCCCACGATCAGTTGAGTTCCGAGG and GACACATATGAAGG -  
874 TCGAAAGAAGGCTCC and inserted into Apal/NdeI sites of pPR2-HA3 (Katris et  
875 al., 2014). The 3' flank was amplified using primers  
876 CTTGCCCCGGGATGGCCTCGCgtaaggaagg and CAGAGCGGCCGCCTGT -  
877 GTCGTGAGCGAGTGAC and then inserted in frame with a Tet7O/SAG4 promoter  
878 using XmaI/NotI sites. Plasmid was linearized with NotI prior to transfection and  
879 selected using pyrimethamine. For ACBP2, flanks were PCR amplified using  
880 respective primers below into the plasmid pPR2-GFP or pPR2-mCherry (adapted  
881 from pPR2-HA3, (Katris et al., 2014). The 5' UTR flank was amplified using  
882 CTGAGGGCCCGCGACGCTCCAGAAGACTCC and GTACCATA -  
883 TGTTATTATATGGTTGAAAGAAGC inserted first using Apal/NdeI sites. Next, the 3'  
884 UTR flank was amplified using GACTGATATCGATT -ACGGCTTCAACTCCGTC and  
885 ATTAGCGGCCGCCTTCATAGGAC -CAGAGCC and inserted using MscI/NotI sites.  
886 ACBP2 cDNA sequence was amplified using  
887 GATCAGATCTAAAATGGCGAGGCCTGTACATCTTGGG and  
888 GTACCCTAGGAGTAGCTTTTGAGGCGGTG inserted last into BglII/AvrII sites then  
889 selected using pyrimethamine. ACBP1 pLIC was PCR amplified using pLIC primers  
890 TACTTCCAATCCAATTTAGCTACAACGGAGCAGACAGAGG and  
891 TCCTCCACTTCCAATTTTAGCCGCGCTTTTCTCGCGCC into pLIC-HA3-CAT  
892 (Sheiner et al., 2011), and linearized prior to transfection and selection on  
893 chloramphenicol.

894 For ACBP1 KO/ACBP2iKD the following protospacer was selected, 5'  
895 GGGGCGTTCCACTGAGAGAA 3', inserted into a U6-Cas9 expression construct  
896 (Sidik et al. 2014). A PCR product w homology flanks for ACBP1 was made with the  
897 following primers 5' ATTTTTTCCAAAGTCCATGCTGGGTTTCTCCCCTG-  
898 TGTCTAGGGAGCCTTAAAACCCTCGAAGGCTGCTAGTAC 3' and

899 5' AGATGATTTGACGACACGCGCCTCGGAAGTCGCTCTGTTTACG-  
900 CGCTTTTTTGCCAGAACACTTGTCAACCG3' using a graCAT-sag-mcherry  
901 resistance cassette as a template and transfected with U6 construct and selected for  
902 with Chloramphenicol. For SCP2 KO/ACBP1iKD, the following protospacer5'  
903 GTACGCTTGCTGTGGAAAAA 3' was inserted into a U6-Cas9 construct and co-  
904 transfected with the following primers 5'

905 gaacaggtgctgacacttgctcgagaatcctgtcgctgcaagttctgagttAAAACCCTCGAAGGCTGCTA  
906 GTAC 3' and 5' agggcgagtttcacgaaatcttctg -  
907 ccaacaaagtgatggtgcagtcgcaTGCCAGAACACTTGTCAACCG 3' using a graCAT-  
908 sag-mcherry resistance cassette and selected for with chloramphenicol.

#### 909 ***T. gondii* transfection**

910 RH-ΔKu80 parasite line was transfected with 100 μg of pLIC-TgATS2-3HA-DHFR  
911 linearized with BlnI for stable integration of HA-tag at C-terminus of TgATS2. 150 μg  
912 pTOXO\_Cas9-CRISPR::gTgATS2-KO and pTOXO\_Cas9-CRISPR::gTgAGPAT-KO  
913 were transfected in TgATS2-HA line with 10 μg of appropriate HXGPRT cassette for  
914 TgATS2-KI and TgATS2-KO, PCR product as described above. Electroporations  
915 were performed in a 2-mm cuvette in a BTX ECM 630 (Harvard Apparatus, at 1,100  
916 V, 25 Ω, and 25 μF. Stable lines expressing the tagged constructs were selected  
917 selected in media with 1 μM pyrimethamine or 25 μg/ml mycophenolic acid and 50  
918 μg/ml xanthine and cloned by limiting dilution.

919 RH-ΔKu80 parasites were also transiently transfected with pLIC-TgAGPAT-3HA-  
920 DHFR. pTOXO\_Cas9-CRISPR::gTgAGPAT-KO was transfected in RH-ΔKu80  
921 parasites for a simple mutant ΔTgAGPAT and in ΔTgATS2 parasites to obtain a  
922 double mutant ΔTgATS2/ΔTgAGPAT. The plasmid pMORN1-CherryRFP-  
923 MORN1/SagCAT were transfected in both RH-ΔKu80 and ΔTgATS2 parasite lines.

924 All other transfections were performed with 50 μg of DNA and electroporation  
925 conditions were as described above. Transfected parasites were incubated at  
926 different concentration with HFF cell 48 h prior to immunofluorescence assay.

#### 927 ***T. gondii* growth assays**

928 **- Plaque Assay:** HFF monolayers were infected with 500 parasites and allowed to  
929 develop for 10 days before staining with Crystal Violet (Sigma) and cell growth  
930 assessment by light microscopy for the presence of intact HFF. To obtain statistical  
931 assessment, each strain was grown in each condition in triplicate and the plaque  
932 area in the same square unit (n=6) are measured. Boxplot with whiskers from  
933 minimum to maximum with median.

**- Cell-based assay:** *T. gondii* growth was determined with an automatic microscope-based screening (Olympus ScanR, Japan). HFFs were seeded at a density of 10,000 cells per well into 96-well plates and were allowed to grow and equilibrate for 48 h at 37°C. Cells were then infected with  $4 \times 10^4$  parasites/well. Invasion was synchronized by briefly centrifugation of plate at 250 g and placed at 37°C for 2 h. The assay was run for 30 h. Hoechst 33342 (Life technologies) stain was then loaded on live cells/parasites at 5 µg/ml for 20 min. Infected cells were fixed with PFA (3.7%) for 10 min at 37°C. A mouse anti-GRA1/Alexa488 labeling (dilution 1:500) was used to identify parasitophorous vacuoles. A total of 20 fields per well were taken using the 20X objective. Images were collected for the distinct fluorescence channels (Hoechst 33342: eg. 360-370 nm, em. 420-460 nm and Alexa488: ex. 460-495, em. 510-550 nm). Images were then analyzed using the ScanR analysis software (Olympus, Tokyo, Japan). For Alexa488 channels images (vacuoles) an intensity algorithm module was used where a fixe threshold was defined with a minimum of 100 pixels size in order to segment the smallest vacuoles (one or two parasite). For Hoechst channel images (parasites nuclei), image process consists to apply a strong background correction and detected parasites with an edge algorithm. A minimum object size of 5 pixels and a maximum object 20 pixels larger one was chosen to discriminate each parasite. ScanR analysis module interface as in flow cytometry allow us to extract and display data as scatter plots and histograms. Using a “gating” procedure we were able to hierarchically filter selected data points with precise boundaries (e.g. number of vacuoles vs number of parasite/vacuoles). The proliferative index was evaluated by parasite/vacuole number ratio. To assess statistically, the samples were prepared in quadruplicate (n=4).

***T. gondii* egress assay:** WT or  $\Delta$ TgATS2 parasites were incubated on HFF cells for approximately 26 h before aspirating medium and replacing with DMEM containing 2 µM A23187 or DMSO in quadruplicate (n=4). Parasites were incubated for 3 min before addition of an equivalent volume of 2x fixative containing 5% Paraformaldehyde, 0.05% glutaraldehyde in PBS (final concentration 2.5% Paraformaldehyde, 0.025% glutaraldehyde). Cells were fixed for 15 min before permeabilizing with 0.025% TritonX100 in PBS for 10 min and then Blocking overnight in blocking solution (2% FBS in PBS). Samples were then probed by immunofluorescence assay and counted manually for egress.

***T. gondii* Red/Green parasite invasion assay:**

Experiment was performed as per (Katris et al., 2014). Parasites were grown for 2 days in quadruplicate (n=4). and harvested intracellular after replacing medium with ENDO buffer (44.7 mM K<sub>2</sub>SO<sub>4</sub>, 10 mM MgSO<sub>4</sub>, 106 mM sucrose, 5 mM glucose, 20 mM Tris-H<sub>2</sub>SO<sub>4</sub>, 3.5 mg/ml BSA, pH 8.2). Cells were scraped, needle passed, filtered and centrifuged at 1800 rpm for 10 min. Cells were resuspended to a concentration of 2.5 x 10<sup>7</sup> cells ml<sup>-1</sup> in ENDO buffer and settled for 20 min onto host cells. Once settled, medium was aspirated and replaced with Invasion buffer (DMEM, 3% FBS and 10 mM HEPES). Parasites were allowed to invade for 15 min before fixation with 2.5% Paraformaldehyde and 0.02% glutaraldehyde. Samples were then blocked in 2% FBS in PBS overnight at 4°C. Samples were probed with mouse anti-SAG1, before washing with PBS, then permeabilized with 0.25% Triton-X100 in PBS. Cells were then probed with rabbit anti-GAP45 and washed in PBS. Samples were then probed with Alexafluor anti-mouse 546 and anti-rabbit 488 before mounting onto slides. Cells were imaged by microscopy and invasion rate determined using ImageJ.

***Plasmodium falciparum* growth assays:**

*P. falciparum* NF54 wild type parasites and FabI-KO (Vaughan et al., 2009) were maintained as previously described (Trager and Jensen, 1976) at 2% haematocrit in RPMI-HEPES supplemented with AlbuMAX II (Gibco). Intra-erythrocytic growth assays in standard media were performed by monitoring the replication of tightly synchronous parasites (5% sorbitol) over four asexual cycles as previously described (Mi-Ichi et al., 2006, Mitamura et al., 2000). Media was replaced daily, sub-culturing were performed every 48 h when required, and parasitemia monitored by Giemsa stained blood smears. Growth assays in lipid-depleted media were performed by synchronizing parasites, before transferring trophozoites to lipid-depleted media as previously reported (Botte et al., 2013, Shears et al., 2017). Briefly, lipid-rich AlbuMAX II was replaced by complementing culture media with an equivalent amount of fatty acid free bovine serum albumin (Sigma), 30 µM palmitic acid (C16:0; Sigma) and 45 µM oleic acid (C18:1; Sigma). All assays were performed in triplicates on different days.

## 998 **Immunofluorescence assay and Microscopy**

999 Parasites were infected to HFF cells grown on coverslips as previously mentioned  
1000 (Amiar et al. 2016). Primary antibodies used: Mouse anti-HA antibody (Roche,  
1001 1:1000), anti CPN60 (1:1000), anti GAP45 (1:1000), rabbit anti-ACP (1:2000), rabbit  
1002 anti-TOM40 (1:3000), polyclonal rabbit anti-IMC1, anti-MIC4 antibodies (1:1000),  
1003 rabbit anti-Sumo21 at (1:500) and mouse anti-Sag1 (1:500), anti-LBPA (1:500) or  
1004 anti-LC3 (1:500). Secondary antibodies: anti-mouse Alexa 488 or 546, anti-rabbit  
1005 Alexa 546- (ThermoFisher Scientific, 1:10000). Mitotracker (1mM) was diluted in  
1006 DMEM 1:5000 (100-300 nM working concentration).

1007 For the immunofluorescence assay (IFA) parasites were grown on confluent HFF on  
1008 coverslips and fixed in PBS containing 2.5% paraformaldehyde (PFA) for 15 min at  
1009 room temperature (RT). Samples were permeabilized with 0.25% Triton X-100 in  
1010 PBS for 10 min at RT prior to blocking in PBS containing 3% BSA and subsequent  
1011 incubation with primary antibodies then secondary antibodies diluted in the blocking  
1012 solution. Labelled parasites were stained with Hoechst (1:10000, ThermoFisher  
1013 Scientific) for 20 min and then washed three times in PBS before final mounting of  
1014 the coverslips on a glass slide using Fluoro-Gel (Electron Microscopy Sciences). The  
1015 fluorescence was visualised using fluorescence microscope (Axio Imager  
1016 2\_apotome; ZEISS) with 63x objective.

## 1017 **Nile red staining of lipid droplets**

1018 The parasites were allowed to infect and growth in confluent monolayer HFF grown  
1019 on coverslips, in the +/- ATc conditions for x days and then fixed in PBS containing  
1020 2.5% paraformaldehyde (PFA) for 15 min at room temperature (RT). Samples were  
1021 permeabilized with 0.25% Triton X-100 in PBS for 10 min at RT and stained with  
1022 primary rat anti-HA antibody followed by detection with secondary AlexaFluor 488-  
1023 conjugated goat anti-rat antibody. Thereafter, the sample coverslips were incubated  
1024 for 1 h with Nile red in 1X. Lastly, three washing steps with 1X PBS were performed  
1025 before proceeding to DNA staining with Hoechst. The coverslips were mounted onto  
1026 a glass slide in fluorogel before proceeding to imaging using fluorescence  
1027 microscope (Axio Imager 2\_apotome; ZEISS). For visualising Nile red stained  
1028 droplets yellow-gold fluorescence (excitation, 450-500 nm; emission, greater than  
1029 528 nm) was used on the Axio imager. Quantification in +/-ATc condition was done  
1030 by counting the no. of lipid droplets per parasite.

#### 1031 **Activity analysis in LPAAT-deficient *E. coli* strains**

1032 Escherichia coli strain deficient in LPAAT/AGPAT activity [SM2-1  $\Delta$ plsC, Coli Genetic  
1033 Stock Center #7587, Yale University] (Coleman, 1990) was used to confirm LPAAT  
1034 activity in both TgATS2 and TgAGPAT.



Coding sequence of *TgATS2* was synthesized (Genscript). *TgAGPAT* coding sequence was amplified by RT-PCR using primer sets 5'-ATGGCGTCCACGCCGCTGC-3'/5'-TTAGAGACCGTGGCCTCGGTG-3' and *TgAGPAT* $\Delta$ N-ter1-72 coding was amplified by RT-PCR using primer sets 5'-CTCAACCGCCCCGCCAGGAATTA-3'/5'-TTAGAGACCGTGGCCTCGGTG-3'. These sequences were digested and ligated into HindIII restriction site on pQE30Xa vector (Quiagen) to generate expression vectors. Additionally, gene coding for *E. coli* LPAAT activity *plsC*, was amplified from *E. coli* DH5alpha genomic DNA using primer sets 5'-CTATATATCTTTTCGTCTTATTATTAC-3'/ 5'-AACTTTTCCGGCGGCTTC-3' and ligated into pQE30Xa vector. Then these acyltransferase vectors and empty pQE30Xa vector as negative control were transfected to electrocompetent cells of SM2-1  $\Delta$ *plsC* deficient *E. coli*. pREP4 repressor vector to regulate Lac promoter activity. Transformed bacterial populations were grown at 37°C in order to promote growth of all isolates. Two independent clones of each bacterial strain that harbours each plasmid-of-interest were isolated for this study. Rescue of LPAAT activity in SM2-1 $\Delta$ *plsC* mutant was measured by the ability to grow at elevated temperature, 42°C, non-permissive temperature in LB medium as previously described (Coleman, 1990). Bacteria were first grown in LB media at 37°C to stationary phase, then the cultures were diluted to OD<sub>600</sub>=0.04 and finally inoculated with several dilutions (at 10<sup>-1</sup> to 10<sup>-6</sup>) on LB plates and incubated for 24 h at permissive (30°C) and non-permissive (42°C) temperatures. All experiments were conducted in triplicate with both independent clones.

#### **Transmission electron microscopy:**

1058 Parasites were grown for 24 h in Labteks (Nunc, Thermofisher) before fixation in 0.1  
1059 M cacodylate buffer with 2.5% glutaraldehyde for 2 h. Samples were then kept in  
1060 fixative. at 4°C until further processing. Sample were then post-fixed 1h with 1%  
1061 osmium tetroxide in cacodylate buffer followed by overnight in 2% uranyl acetate in  
1062 distilled water. After dehydration in graded series of acetonitrile, samples were  
1063 progressively impregnated in Epon812, the wells were then filled with fresh resin and  
1064 allowed to polymerize 48 h at 60°C. Ultrathin 70 nm section were obtained with a  
1065 Leica UCT Ultramicrotome and collected on copper grids. Grids were post-stained  
1066 with uranyl acetate and lead citrate before their observation on a Jeol1200EXII  
1067 Transmission Electron Microscope. All chemicals were from Electron Microscopy  
1068 Sciences.

#### 1069 **Lipidomic analysis by GCMS extraction from *T. gondii* tachyzoites**

1070 Lipid extraction and analysis of tachyzoites was performed as previously described  
1071 (Ramakrishnan et al., 2012, Amiar et al., 2016, Dubois et al., 2018). Freshly  
1072 egressed tachyzoites ( $1 \times 10^8$  cell equivalents) grown in standard culture (n=4) or in  
1073 starvation culture (n=3), were metabolically quenched by rapid chilling of the cell  
1074 suspension in a dry ice/ethanol bath and lipids were extracted in  
1075 chloroform/methanol/water (2:1:0.8, v/v/v containing 25 nmol tridecanoic acid C13:0  
1076 as extraction internal standard) for total lipid analysis.

1077 **- For lipid quantification:** Total lipid extraction was performed as described  
1078 previously (Amiar et al., 2016). Parasites were prepared as described above except  
1079 for the addition of 0.1 M of HCl to promote PA and LPA extraction. Pooled organic  
1080 phase was subjected to biphasic separation by adding 0.1 M HCl. In both protocols,  
1081 the organic phase was dried with speed vacuum and dissolved in 1-butanol.

1082 **- Total lipids analysis:** An aliquot of the lipid extract was dried in vacuum  
1083 concentrator with 1 nmol pentadecanoic acid C15:0 as internal standard. Then the  
1084 dried lipid was dissolved in the chloroform/methanol, (2:1, v/v) and derivatised with  
1085 MethPrep II (Alltech). The resulting fatty acid methyl esters was analysed by GC-MS  
1086 as described previously (Amiar et al., 2016). Fatty acid methyl esters were identified  
1087 by their mass spectrum and retention time compared to authentic standards. Lipid  
1088 data was analysed using Agilent® Masshunter software.

**- Lipid quantification:** Total lipid fraction was separated by 2D-HPTLC (Merck) with 5 µg PA(C17:0/C17:0) and 5 µg LPA(C17:0) (Avanti Polar lipids) using chloroform/methanol/28% NH<sub>4</sub>OH, 60:35:8 (v/v) as the 1st dimension solvent system and chloroform/acetone/methanol/acetic acid/water, 50:20:10:13:5 (v/v/v/v/v) as the 2nd dimension solvent system (Amiar et al., 2016). For DAG analysis, total lipid fraction was separated by 1D-HPTLC using hexane/diethylether/formic acid, 80:20:2 (v/v/v) as solvent system. The spot on the HPTLC corresponding to each lipid was scrapped off and lipids were directly derivatised with 0.5 M methanoic HCl in the presence of 1 nmol pentadecanoic acid (C15:0) as internal standard. The resulting fatty acid methyl esters were extracted with hexane and analysed by GC-MS (Amiar et al., 2016). Resulted FAME and cholesterol-TMS was analyzed by GC-MS (5977A-7890B, Agilent). FAME was then quantified using Mass Hunter Quantification software (Agilent). All statistical analyses were conducted using GraphPad Prism software. P values of  $\leq 0.05$  from statistical analyses (Ttests) were considered statistically significant.

#### **Stable isotope labelling of *T. gondii***

Stable isotope labelling using U-<sup>13</sup>C-glucose (Cambridge Isotope Laboratories, USA), lipid extraction, and GC-MS analysis was performed as previously described (Ramakrishnan et al., 2012, Amiar et al., 2016). Freshly infected HFF were incubated in glucose-free medium supplemented with 8 mM U-<sup>13</sup>C-glucose. For FBS starvation study, 5% FBS was add to U-<sup>13</sup>C-glucose medium in standard culture conditions and 1% FBS was add to U-<sup>13</sup>C-glucose medium in starvation culture condition. Parasites were harvested 72 h post-infection and metabolites extracted as above.

#### **Phospholipid import assay:**

Freshly lysed cultures of WT or  $\Delta$ TgATS2 parasites (n=3) were harvested, filtered and resuspended in DMEM to a concentration of approximately  $2 \times 10^8$  cells ml<sup>-1</sup>. Cells were then mixed with a 2x solution containing 10 $\mu$ g ml<sup>-1</sup> NBD-PA or NBD-PC (5  $\mu$ g/mL final) and incubated at 37°C. Parasites were then spun down, resuspended in PBS. PFA was then added to a final concentration of 2.5%, and cells were fixed for 15 min before being spun down again and resuspended in 1xPBS. Parasites were smeared onto polyethyleneimine coated coverslips, and then probed with anti-SAG1 primary (1:1000) and anti-mouse Alexa 546 secondary antibodies (1:10000) by immunofluorescence microscopy, stained with DAPI (1:10000) and mounted onto slides. Samples were imaged by microscopy. SAG1 labelling was used to identify parasites using ImageJ and then estimate the amount of NBD-lipid uptaken by the parasites.

#### **D Quantification and statistical analysis**

Statistical analyses for all experiments were performed with Prism software v7 (GraphPad). In experiments comparing only two groups, t-test with Holm-Sidak correction were used to compare the experimental group with the control group. For other experiments including 3 groups, non-parametric ANOVA tests (Sidak correction for multiple tests) were used. Individual p values are indicated in each figure. Each experiment was done in n=3 otherwise mentioned in material methods. For lipidomic analysis, Agilent® Masshunter software, was used for fatty acid analysis and subjected to statistical analysis as described above.

#### **d DATA AND CODE AVAILABILITY**

No unique code or software was generated in this study. All datasets generated and analysed during this study are available upon request to the lead contact Cyrille Botte (cyrille.botte@univ-grenoble-alpes.fr).

#### **Abbreviations:**

FA, fatty acid; FASII, fatty acid synthesis; PL, phospholipid; PC, phosphatidylcholine; PE, phosphatidylethanolamine; PS, phosphatidylserine; PI, phosphatidylinositol; TAG, triacylglycerol; PA, phosphatidic acid; GPAT, glycerol-3-phosphate acyltransferase; LPA, lysophosphatidic acid; AGPAT, acyl-glycerol3-phosphate

acyltransferase; Drp, dynamin related protein; PVM, parasitophorous vacuole membrane; KI, knock-in; KO, knock-out; IMC, inner membrane complex; IFA, immunofluorescent assay; PM, plasma membrane; EM, electron microscopy; DAG, diacylglycerol; CL, cardiolipin; FBS, foetal bovine serum; HFF, human foreskin fibroblast; ACP, acyl-CoA binding protein; gMVB, giant multi vesicular body; LBPA, lysobisphosphatidic acid; ACP, acyl carrier protein; IPP, isopentenylphosphate

## References

- ADACHI, Y., IJIMA, M. & SESAHI, H. 2018. An unstructured loop that is critical for interactions of the stalk domain of Drp1 with saturated phosphatidic acid. *Small GTPases*, 9, 472-479.
- ADACHI, Y., ITOH, K., YAMADA, T., CERVENY, K. L., SUZUKI, T. L., MACDONALD, P., FROHMAN, M. A., RAMACHANDRAN, R., IJIMA, M. & SESAHI, H. 2016. Coincident Phosphatidic Acid Interaction Restrains Drp1 in Mitochondrial Division. *Mol Cell*, 63, 1034-43.
- AMIAR, S., MACRAE, J. I., CALLAHAN, D. L., DUBOIS, D., VAN DOOREN, G. G., SHEARS, M. J., CESBRON-DELAUW, M.-F., MARÉCHAL, E., MCCONVILLE, M. J., MCFADDEN, G. I., YAMARYO-BOTTE, Y. & BOTTE, C. Y. 2016. Apicoplast-Localized Lysophosphatidic Acid Precursor Assembly Is Required for Bulk Phospholipid Synthesis in *Toxoplasma gondii* and Relies on an Algal/Plant-Like Glycerol 3-Phosphate Acyltransferase. *PLoS Pathogens*, 12, e1005765.
- BISANZ, C., BASTIEN, O., GRANDO, D., JOUHET, J., MARECHAL, E. & CESBRON-DELAUW, M. F. 2006. *Toxoplasma gondii* acyl-lipid metabolism: de novo synthesis from apicoplast-generated fatty acids versus scavenging of host cell precursors. *Biochem J*, 394, 197-205.
- BOTTE, C. Y., YAMARYO-BOTTE, Y., RUPASINGHE, T. W., MULLIN, K. A., MACRAE, J. I., SPURCK, T. P., KALANON, M., SHEARS, M. J., COPPEL, R. L., CRELLIN, P. K., MARECHAL, E., MCCONVILLE, M. J. & MCFADDEN, G. I. 2013. Atypical lipid composition in the purified relict plastid (apicoplast) of malaria parasites. *Proc Natl Acad Sci U S A*, 110, 7506-11.
- BOUGDOUR, A., TARDIEUX, I. & HAKIMI, M. A. 2014. *Toxoplasma* exports dense granule proteins beyond the vacuole to the host cell nucleus and rewires the host genome expression. *Cell Microbiol*, 16, 334-43.
- BREINICH, M. S., FERGUSON, D. J., FOTH, B. J., VAN DOOREN, G. G., LEBRUN, M., QUON, D. V., STRIEPEN, B., BRADLEY, P. J., FRISCHKNECHT, F., CARRUTHERS, V. B. & MEISSNER, M. 2009. A dynamin is required for the biogenesis of secretory organelles in *Toxoplasma gondii*. *Curr Biol*, 19, 277-86.
- BROWN, W. J., PLUTNER, H., DRECKTRAH, D., JUDSON, B. L. & BALCH, W. E. 2008. The lysophospholipid acyltransferase antagonist CI-976 inhibits a late step in COPII vesicle budding. *Traffic (Copenhagen, Denmark)*, 9, 786-797.
- BURGER, K. N. J., DEMEL, R. A., SCHMID, S. L. & DE KRUIJFF, B. 2000. Dynamin Is Membrane-Active: Lipid Insertion Is Induced by Phosphoinositides and Phosphatidic Acid  $\dagger$ . *Biochemistry*, 39, 12485-12493.
- COLEMAN, J. 1990. Characterization of *Escherichia coli* cells deficient in 1-acyl-sn-glycerol-3-phosphate acyltransferase activity. *J Biol Chem*, 265, 17215-21.
- COSTA, G., GILDENHARD, M., ELDERING, M., LINDQUIST, R. L., HAUSER, A. E., SAUERWEIN, R., GOOSMANN, C., BRINKMANN, V., CARRILLO-BUSTAMANTE, P. & LEVASHINA, E. A. 2018. Non-competitive resource exploitation within mosquito shapes within-host malaria infectivity and virulence. *Nat Commun*, 9, 3474.
- DAILY, J. P., SCANFELD, D., POCHET, N., LE ROCH, K., PLOUFFE, D., KAMAL, M., SARR, O., MBOUP, S., NDIR, O., WYPIJ, D., LEVASSEUR, K., THOMAS, E., TAMAYO, P., DONG, C., ZHOU, Y., LANDER, E. S., NDIAYE, D., WIRTH, D., WINZELER, E. A., MESIROV, J. P. & REGEV, A. 2007. Distinct

physiological states of *Plasmodium falciparum* in malaria-infected patients. *Nature*, 450, 1091-1095.

DEREEPER, A., GUIGNON, V., BLANC, G., AUDIC, S., BUFFET, S., CHEVENET, F., DUFAYARD, J.-F., GUINDON, S., LEFORT, V., LESCOT, M., CLAVERIE, J.-M. & GASCUEL, O. 2008. Phylogeny.fr: robust phylogenetic analysis for the non-specialist. *Nucleic acids research*, 36, W465-9.

DUBOIS, D., FERNANDES, S., AMIAR, S., DASS, S., KATRIS, N. J., BOTTE, C. Y. & YAMARYO-BOTTE, Y. 2018. Toxoplasma gondii acetyl-CoA synthetase is involved in fatty acid elongation (of long fatty acid chains) during tachyzoite life stages. *J Lipid Res*, 59, 994-1004.

FRANCO, M., PANAS, M. W., MARINO, N. D., LEE, M. C., BUCHHOLZ, K. R., KELLY, F. D., BEDNARSKI, J. J., SLECKMAN, B. P., POURMAND, N. & BOOTHROYD, J. C. 2016. A Novel Secreted Protein, MYR1, Is Central to Toxoplasma's Manipulation of Host Cells. *MBio*, 7, e02231-15.

GRAS, S., JIMENEZ-RUIZ, E., KLINGER, C. M., SCHNEIDER, K., KLINGL, A., LEMGRUBER, L. & MEISSNER, M. 2019. An endocytic-secretory cycle participates in Toxoplasma gondii in motility. *PLOS Biology*, 17, e3000060.

GUINDON, S., DUFAYARD, J. F., LEFORT, V., ANISIMOVA, M., HORDIJK, W. & GASCUEL, O. 2010. New algorithms and methods to estimate maximum-likelihood phylogenies: assessing the performance of PhyML 3.0. *Syst Biol*, 59, 307-21.

GULATI, S., EKLAND, E. H., RUGGLES, K. V., CHAN, R. B., JAYABALASINGHAM, B., ZHOU, B., MANTEL, P. Y., LEE, M. C., SPOTTISWOODE, N., COBURN-FLYNN, O., HJELMQVIST, D., WORGALL, T. S., MARTI, M., DI PAOLO, G. & FIDOCK, D. A. 2015. Profiling the Essential Nature of Lipid Metabolism in Asexual Blood and Gametocyte Stages of *Plasmodium falciparum*. *Cell Host Microbe*, 18, 371-81.

HEREDERO-BERMEJO, I., VARBERG, J. M., CHARVAT, R., JACOBS, K., GARBUZ, T., SULLIVAN JR., W. J. & ARRIZABALAGA, G. 2019. TgDrpC, an atypical dynamin-related protein in *Toxoplasma gondii*, is associated with vesicular transport factors and parasite division. *Molecular Microbiology*, 111, 46-64.

HU, X., BINNS, D. & REESE, M. L. 2017. The coccidian parasites *Toxoplasma* and *Neospora* dysregulate mammalian lipid droplet biogenesis. *J Biol Chem*, 292, 11009-11020.

HUYNH, M. H. & CARRUTHERS, V. B. 2009. Tagging of endogenous genes in a *Toxoplasma gondii* strain lacking Ku80. *Eukaryot Cell*, 8, 530-9.

JANOUSKOVEC, J., HORÁK, A., OBORNÍK, M., LUKEŠ, J. & KEELING, P. J. 2010. A common red algal origin of the apicomplexan, dinoflagellate, and heterokont plastids. *Proceedings of the National Academy of Sciences of the United States of America*, 107, 10949-10954.

KATRIS, N. J., VAN DOOREN, G. G., MCMILLAN, P. J., HANSEN, E., TILLEY, L. & WALLER, R. F. 2014. The apical complex provides a regulated gateway for secretion of invasion factors in *Toxoplasma*. *PLoS Pathog*, 10, e1004074.

KIM, K., SOLDATI, D. & BOOTHROYD, J. C. 1993. Gene replacement in *Toxoplasma gondii* with chloramphenicol acetyltransferase as selectable marker. *Science*, 262, 911-4.

KOBAYASHI, T., STANG, E., FANG, K. S., DE MOERLOOSE, P., PARTON, R. G. & GRUENBERG, J. 1998. A lipid associated with the antiphospholipid syndrome regulates endosome structure and function. *Nature*, 392, 193-7.

KOOIJMAN, E. E., CHUPIN, V., FULLER, N. L., KOZLOV, M. M., DE KRUIJFF, B., BURGER, K. N. J. & RAND, P. R. 2005. Spontaneous curvature of phosphatidic acid and lysophosphatidic acid. *Biochemistry*, 44, 2097-2102.

LARKIN, M. A., BLACKSHIELDS, G., BROWN, N. P., CHENNA, R., MCGETTIGAN, P. A., MCWILLIAM, H., VALENTIN, F., WALLACE, I. M., WILM, A., LOPEZ, R., THOMPSON, J. D., GIBSON, T. J. & HIGGINS, D. G. 2007. Clustal W and Clustal X version 2.0. *Bioinformatics*, 23, 2947-8.

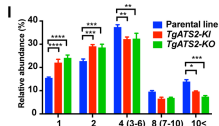
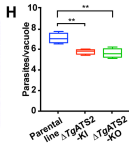
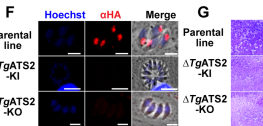
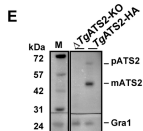
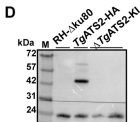
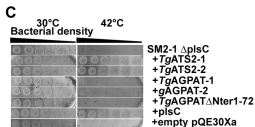
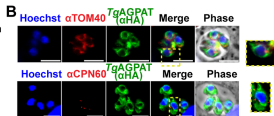
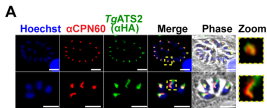
LI, W., COWLEY, A., ULUDAG, M., GUR, T., MCWILLIAM, H., SQUIZZATO, S., PARK, Y. M., BUSO, N. & LOPEZ, R. 2015. The EMBL-EBI bioinformatics web and programmatic tools framework. *Nucleic Acids Res*, 43, W580-4.

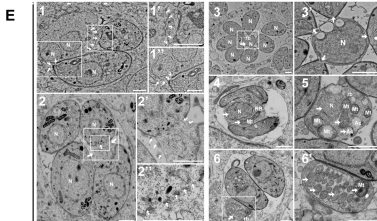
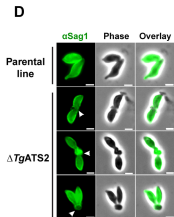
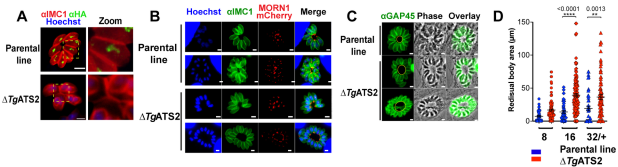
MACRAE, J. I., MARECHAL E FAU - BIOT, C., BIOT C FAU - BOTTE, C. Y. & BOTTE, C. Y. 2012. The apicoplast: a key target to cure malaria.

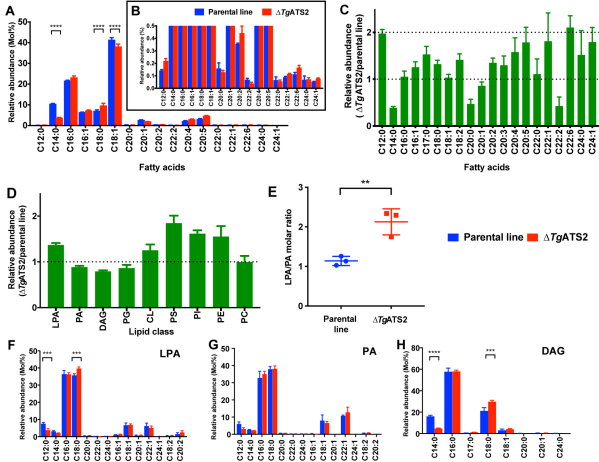
- MANCIO-SILVA, L., SLAVIC, K., GRILO RUIVO, M. T., GROSSO, A. R., MODRZYNSKA, K. K., VERA, I. M., SALES-DIAS, J., GOMES, A. R., MACPHERSON, C. R., CROZET, P., ADAMO, M., BAENA-GONZALEZ, E., TEWARI, R., LLINAS, M., BILLKER, O. & MOTA, M. M. 2017. Nutrient sensing modulates malaria parasite virulence. *Nature*, 547, 213-216.
- MARTINS-DUARTE, E. S., DUBAR, F., LAWTON, P., DA SILVA, C. F., SOEIRO MDE, N., DE SOUZA, W., BIOT, C. & VOMMARO, R. C. 2015. Ciprofloxacin Derivatives Affect Parasite Cell Division and Increase the Survival of Mice Infected with *Toxoplasma gondii*. *PLoS One*, 10, e0125705.
- MAZUMDAR, J., E, H. W., MASEK, K., C, A. H. & STRIEPEN, B. 2006. Apicoplast fatty acid synthesis is essential for organelle biogenesis and parasite survival in *Toxoplasma gondii*. *Proc Natl Acad Sci U S A*, 103, 13192-7.
- MELATTI, C., PIEPERHOFF, M., LEMGRUBER, L., POHL, E., SHEINER, L. & MEISSNER, M. 2019. A unique dynamin-related protein is essential for mitochondrial fission in *Toxoplasma gondii*. *PLOS Pathogens*, 15, e1007512.
- MENARD, D. & DONDORP, A. 2017. Antimalarial Drug Resistance: A Threat to Malaria Elimination. *Cold Spring Harbor Perspectives in Medicine*, 7.
- MI-ICHI, F., KANO, S. & MITAMURA, T. 2007. Oleic acid is indispensable for intraerythrocytic proliferation of *Plasmodium falciparum*. *Parasitology*, 134.
- MI-ICHI, F., KITA, K. & MITAMURA, T. 2006. Intraerythrocytic *Plasmodium falciparum* utilize a broad range of serum-derived fatty acids with limited modification for their growth. *Parasitology*, 133, 399-410.
- MITAMURA, T., HANADA, K., KO-MITAMURA, E. P., NISHIJIMA, M. & HORII, T. 2000. Serum factors governing intraerythrocytic development and cell cycle progression of *Plasmodium falciparum*. *Parasitol Int*, 49, 219-29.
- MUELLER, C., KLAGES, N., JACOT, D., SANTOS, J. M., CABRERA, A., GILBERGER, T. W., DUBREMETZ, J.-F. & SOLDATI-FAVRE, D. 2013. The *Toxoplasma* protein ARO mediates the apical positioning of rhoptry organelles, a prerequisite for host cell invasion. *Cell host & microbe*, 13, 289-301.
- NOLAN, S. J., ROMANO, J. D. & COPPENS, I. 2017. Host lipid droplets: An important source of lipids salvaged by the intracellular parasite *Toxoplasma gondii*. *PLoS Pathog*, 13, e1006362.
- OHLROGGE, J. & BROWSE, J. 1995. Lipid biosynthesis. *Plant Cell*, 7, 957-70.
- PERNAS, L., ADOMAKO-ANKOMAH, Y., SHASTRI, A. J., EWALD, S. E., TREECK, M., BOYLE, J. P. & BOOTHROYD, J. C. 2014. *Toxoplasma* Effector MAF1 Mediates Recruitment of Host Mitochondria and Impacts the Host Response. *PLOS Biology*, 12, e1001845.
- RAMAKRISHNAN, S., DOCAMPO, M. D., MACRAE, J. I., PUJOL, F. M., BROOKS, C. F., VAN DOOREN, G. G., HILTUNEN, J. K., KASTANIOTIS, A. J., MCCONVILLE, M. J. & STRIEPEN, B. 2012. Apicoplast and endoplasmic reticulum cooperate in fatty acid biosynthesis in apicomplexan parasite *Toxoplasma gondii*. *J Biol Chem*, 287, 4957-4971.
- ROMANO, J. D., NOLAN, S. J., PORTER, C., EHRENMAN, K., HARTMAN, E. J., HSIA, R. C. & COPPENS, I. 2017. The parasite *Toxoplasma* sequesters diverse Rab host vesicles within an intravacuolar network. *J Cell Biol*, 216, 4235-4254.
- SCHMIDT, A., WOLDE, M., THIELE, C., FEST, W., KRATZIN, H., PODTELEJNIKOV, A. V., WITKE, W., HUTTNER, W. B. & SOLING, H. D. 1999. Endophilin I mediates synaptic vesicle formation by transfer of arachidonate to lysophosphatidic acid. *Nature*, 401, 133-41.
- SHEARS, M. J., MACRAE, J. I., MOLLARD, V., GOODMAN, C. D., STURM, A., ORCHARD, L. M., LLINAS, M., MCCONVILLE, M. J., BOTTE, C. Y. & MCFADDEN, G. I. 2017. Characterization of the *Plasmodium falciparum* and *P. berghei* glycerol 3-phosphate acyltransferase involved in FASII fatty acid utilization in the malaria parasite apicoplast. *Cell Microbiol*, 19.
- SHEINER, L., DEMERLY, J. L., POULSEN, N., BEATTY, W. L., LUCAS, O., BEHNKE, M. S., WHITE, M. W. & STRIEPEN, B. 2011. A Systematic Screen to Discover and Analyze Apicoplast Proteins Identifies a Conserved and Essential Protein Import Factor. *PLoS Pathogens*, 7, e1002392.
- SHIN, J. J. H. & LOEWEN, C. J. R. 2011. Putting the pH into phosphatidic acid signaling. *BMC biology*, 9, 85.

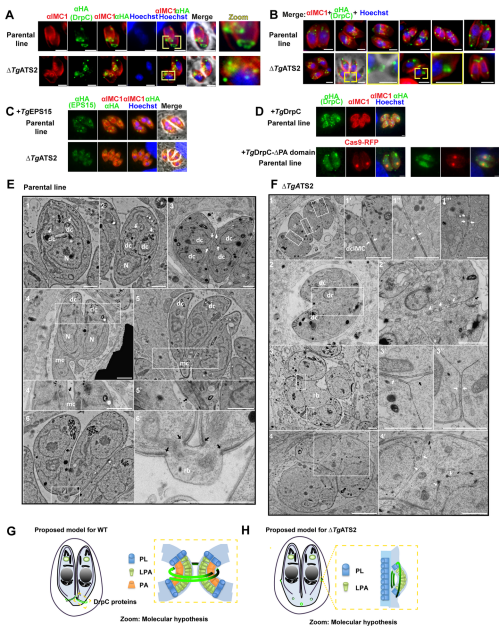
- SIDIK, S. M., HACKETT, C. G., TRAN, F., WESTWOOD, N. J. & LOURIDO, S. 2014. Efficient genome engineering of *Toxoplasma gondii* using CRISPR/Cas9. *PLoS ONE*, 9, e100450.
- SIDIK, S. M., HUET, D., GANESAN, S. M., HUYNH, M. H., WANG, T., NASAMU, A. S., THIRU, P., SAEIJ, J. P. J., CARRUTHERS, V. B., NILES, J. C. & LOURIDO, S. 2016. A Genome-wide CRISPR Screen in *Toxoplasma* Identifies Essential Apicomplexan Genes. *Cell*, 166, 1423-1435.e12.
- UBOLDI, A. D., MCCOY, J. M., BLUME, M., GERLIC, M., FERGUSON, D. J., DAGLEY, L. F., BEAHAN, C. T., STAPLETON, D. I., GOOLEY, P. R., BACIC, A., MASTERS, S. L., WEBB, A. I., MCCONVILLE, M. J. & TONKIN, C. J. 2015. Regulation of Starch Stores by a Ca(2+)-Dependent Protein Kinase Is Essential for Viable Cyst Development in *Toxoplasma gondii*. *Cell Host Microbe*, 18, 670-81.
- VAN DOOREN, G. G., REIFF, S. B., TOMOVA, C., MEISSNER, M., HUMBEL, B. M. & STRIEPEN, B. 2009. A novel dynamin-related protein has been recruited for apicoplast fission in *Toxoplasma gondii*. *Curr Biol*, 19, 267-76.
- VAUGHAN, A. M., O'NEILL, M. T., TARUN, A. S., CAMARGO, N., PHUONG, T. M., ALY, A. S. I., COWMAN, A. F. & KAPPE, S. H. I. 2009. Type II fatty acid synthesis is essential only for malaria parasite late liver stage development. *Cell Microbiol*, 11, 506-520.
- WALLER, R. F., KEELING, P. J., DONALD, R. G., STRIEPEN, B., HANDMAN, E., LANG-UNNASCH, N., COWMAN, A. F., BESRA, G. S., ROOS, D. S. & MCFADDEN, G. I. 1998. Nuclear-encoded proteins target to the plastid in *Toxoplasma gondii* and *Plasmodium falciparum*. *Proc Natl Acad Sci U S A*, 95, 12352-12357.
- WELTI, R., MUI, E., SPARKS, A., WERNIMONT, S., ISAAC, G., KIRISITS, M., ROTH, M., ROBERTS, C. W., BOTTE, C., MARECHAL, E. & MCLEOD, R. 2007. Lipidomic analysis of *Toxoplasma gondii* reveals unusual polar lipids. *Biochemistry*, 46, 13882-90.
- YEH, E. & DERISI, J. L. 2011. Chemical rescue of malaria parasites lacking an apicoplast defines organelle function in blood-stage *Plasmodium falciparum*. *PLoS Biol*, 9, e1001138.
- YLÄ-ANTTILA, P., VIHINEN, H., JOKITALO, E. & ESKELINEN, E. L. 2009. Chapter 10 Monitoring Autophagy by Electron Microscopy in Mammalian Cells. *Methods in Enzymology*. Academic Press.
- YU, M., KUMAR, T. R., NKRUMAH, L. J., COPPI, A., RETZLAFF, S., LI, C. D., KELLY, B. J., MOURA, P. A., LAKSHMANAN, V., FREUNDLICH, J. S., VALDERRAMOS, J. C., VILCHEZE, C., SIEDNER, M., TSAI, J. H., FALKARD, B., SIDHU, A. B., PURCELL, L. A., GRATRAUD, P., KREMER, L., WATERS, A. P., SCHIEHSE, G., JACOBUS, D. P., JANSE, C. J., AGER, A., JACOBS, W. R., JR., SACCHETTINI, J. C., HEUSSLER, V., SINNIS, P. & FIDOCK, D. A. 2008. The fatty acid biosynthesis enzyme FabI plays a key role in the development of liver-stage malarial parasites. *Cell Host Microbe*, 4, 567-78.
- ZHANG, M., WANG, C., OTTO, T. D., OBERSTALLER, J., LIAO, X., ADAPA, S. R., UDENZE, K., BRONNER, I. F., CASANDRA, D., MAYHO, M., BROWN, J., LI, S., SWANSON, J., RAYNER, J. C., JIANG, R. H. Y. & ADAMS, J. H. 2018. Uncovering the essential genes of the human malaria parasite *Plasmodium falciparum* by saturation mutagenesis. *Science*, 360.
- ZUZARTE-LUIS, V., MELLO-VIEIRA, J., MARREIROS, I. M., LIEHL, P., CHORA, A. F., CARRET, C. K., CARVALHO, T. & MOTA, M. M. 2017. Dietary alterations modulate susceptibility to *Plasmodium* infection. *Nat Microbiol*, 2, 1600-1607.

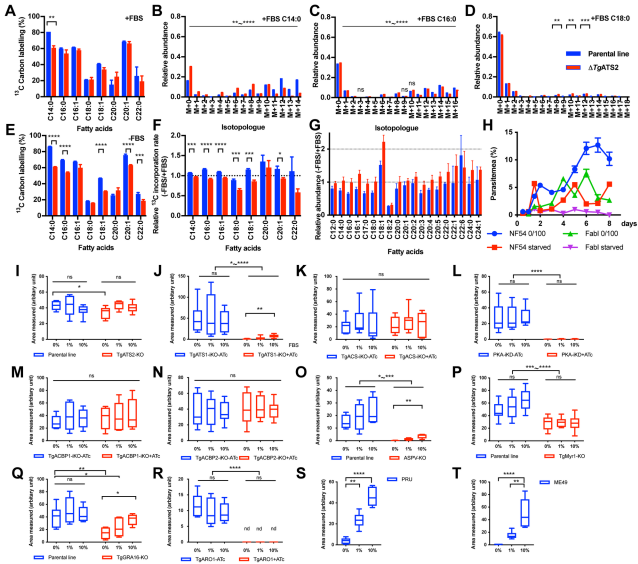






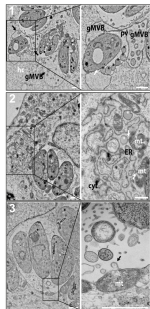




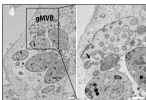


## A Parental line

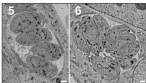
### 0% FBS



### 1% FBS

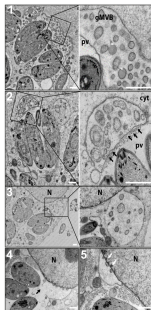


### 10% FBS

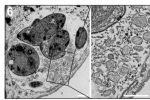


## B $\Delta TgATS2$

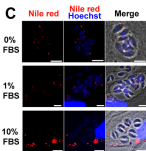
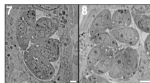
### 0% FBS



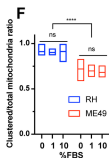
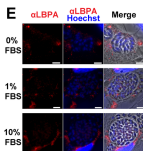
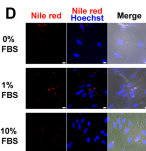
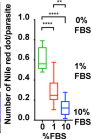
### 1% FBS



### 10% FBS



Number of Nile red dot/parasite

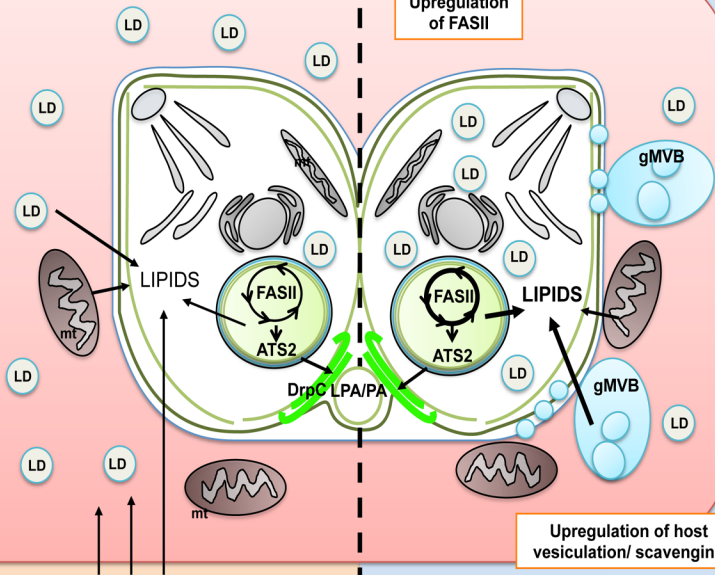


[illegible][illegible]

## Lipid rich environment

## Lipid starved environment

Host cell



Nutrients / Fatty acids / Lipids